Cargo-Loading of Misfolded Proteins into Extracellular Vesicles: The Role of J Proteins

Desmond Pink[2], Julien Donnelier[1], John Lewis[2,3] and Janice E.A. Braun[1]**

[1] Hotchkiss Brain Institute, Department of Biochemistry and Molecular Biology, Cumming School of Medicine, University of Calgary, Calgary, Alberta, Canada
[2]Nanostics Precision Health, Edmonton, Alberta, Canada
[3]Department of Oncology, University of Alberta, Edmonton, Alberta, Canada

** To whom correspondence should be addressed

Janice E.A. Braun, Ph.D. M.Sc.
Hotchkiss Brain Institute
Department of Biochemistry and Molecular Biology
Cumming School of Medicine, University of Calgary
3330 Hospital Dr. N.W.
Calgary, Alberta, Canada T2N 4N1
Office (403) 220-5463
Lab (403) 220-2190
FAX (403) 210-7446
http://www.ucalgary.ca/~braunj/index.html

Abstract

Extracellular vesicles (EVs) are a collection of secreted vesicles of diverse size and cargo that are implicated in the physiological removal of nonfunctional proteins as well as the cell-to-cell transmission of disease-causing-proteins in several neurodegenerative diseases. We have shown that the molecular chaperone, cysteine string protein (CSPα; DnaJC5), is responsible for the export of disease-causing-misfolded proteins from neurons via EVs. We show here that CSPα-EVs efficiently deliver GFP-tagged 72Q huntingtin^{exon1} to naive neurons. When we analyzed the heterogeneous EV pool, we found that the misfolded GFP-tagged 72Q huntingtin^{exon1} cargo was primarily found in EVs between 180-240nm. We further determined that cargo-loading of GFP-tagged 72Q huntingtin^{exon1} into EVs was impaired by resveratrol. Importantly, in addition to CSPα, we identified two other J protein co-chaperones, DnaJB2 and DnaJB6, that facilitate EV export of GFP-tagged 72Q huntingtin^{exon1}. While human mutations in CSPα cause the neurodegenerative disorder, adult neuronal ceroid lipofuscinosis, mutations in DnaJB6 cause limb-girdle muscular dystrophy and mutations in DnaJB2 are linked to the neurodegenerative disorders, Charcot Marie Tooth disease, distal hereditary motor neuropathy, spinal muscular atrophy and juvenile Parkinsonism. Our data provides new insights into the parallels between proteostasis and EV export, as three J proteins linked to disease in humans are the same as those that mediate EV genesis and export of misfolded proteins.

Introduction

The cell-to-cell transfer of extracellular vesicles (EVs) is a conserved process. *In vivo,* the continuous exchange among different cells generates a dynamic and heterogeneous pool of EVs [46]. EVs come in different sizes and carry different cargoes that exert profound effects in recipient cells following uptake. The physiological roles of EVs are still ill-defined but include exchanging physiological information between cells as well as removing unwanted proteins from cells [39,46,72]. EVs are also implicated in disease progression. How EVs facilitate the spread of disease in cancer and neurodegenerative disease and what distinguishes physiological from pathological EVs is a current focus of investigation [36,72]. While complex cargoes of DNA, RNA, proteins, lipids and metabolites are packaged in EVs for delivery to recipient cells, our understanding of the mechanisms that target proteins to EVs is rudimentary in comparison to the conventional secretory pathway. We have recently identified an EV protein-sorting pathway, the CSPα-EV export pathway, that exports misfolded disease-causing proteins from neurons [15]. These findings are consistent with those of Fontaine and colleagues who also report the export of disease-causing proteins via this pathway [22]. We found that the molecular co-chaperone, CSPα (cysteine string protein, DnaJC5) promotes EV export of distinct misfolded disease-causing proteins and that this export pathway is 'druggable' as demonstrated by the ability of the polyphenol, resveratrol, to block CSPα-mediated export of misfolded proteins [15]. Resveratrol was initially linked to CSPα function in a chemical screen as a compound that alters life span of CSPα *c. elegans* mutants [41].

Cysteine string protein (CSPα, DnaJC5) is a presynaptic co-chaperone that is critical for synaptic proteostasis [6,20]. It is a central player in the synapse-specific machinery that protects against local proteostasis imbalances at the synapse which can lead to neurotransmission deficits, accumulation of misfolded, nonfunctional proteins, synaptic loss and neurodegeneration. Human mutations in CSPα, L115R and L116Δ, cause the neurodegenerative disorder adult neuronal ceroid lipofuscinosis (ANCL) [3,54,70]. Deletion of CSPα leads to neurodegeneration in multiple experimental models. CSPα knock-out mice exhibit fulminant neurodegeneration and have a reduced lifespan with no mice surviving beyond 3 months [20]. Loss-of-function CSPα *Drosophila* mutants demonstrate uncoordinated movements, temperature-sensitive paralysis and early lethality [77]. And, in *C elegans*, CSPα null mutants display neurodegeneration and reduced lifespan [42]. Not surprisingly, CSPα dysfunction has been implicated in several neurodegenerative disorders in addition to ANCL, including Alzheimer's, Parkinson's and Huntington's disease [7,16,34,50,69,76]. CSPα is a member of the large J Protein (DnaJ) co-chaperone family [40]. J proteins are Hsp70-interacting proteins that have diverse roles in proteostasis. Disruption or absence of a number of different J proteins is known to compromise neuronal function [38,43,75].

Collectively, this work suggests that CSPα may contribute to proteostasis by exporting misfolded proteins in EVs for off-site disposal in recipient cells. This hypothesis predicts that in the absence of an EV export pathway, misfolded proteins accumulate and neurodegeneration occurs in donor cells. The hypothesis further predicts that dysregulated disposal of misfolded proteins by recipient cells may trigger toxic protein spreading or neurodegeneration. To begin to study these possibilities, we explored two aspects of the CSPα-EV export pathway: (i) whether the molecule resveratrol inhibits secretion of EVs in general, or CSPαEVs selectively

and (ii) whether members of the J protein co-chaperone family, other than CSPα, export misfolded proteins such as GFP-72Q huntingtin^{exon1}. Our results confirm and extend our previous findings. We show that within the heterogeneous EV population released from CAD cells, the 180-240nm subpopulation of EVs predominantly contain the GFP-tagged 72Q huntingtin^{exon1} cargo, and that CSPα increases secretion of this EV subpopulation. Moreover, we find that resveratrol impairs cargo-loading of CSPα-EVs. We further demonstrate that, in addition to the CSPα-EV pathway, misfolded proteins can be secreted via the DnaJB2- and DnaJB6-EV export pathways. CSPα-, DnaJB2- as well as DnaJB6-EVs are delivery competent in that they transfer misfolded GFP-72Q huntingtin cargo to recipient cells. Our data highlight a role of signal sequence lacking-co-chaperones in the sorting of misfolded cargo into specific EVs for export and demonstrate that this EV transit pathway can be targeted pharmacologically.

Results

The CSPα EV export pathway

Trinucleotide repeat expansions of the huntingtin gene cause Huntington's disease, a progressive neurodegenerative disorder that manifests in midlife [31]. Aggregates of polyglutamine-expanded huntingtin are found within genetically normal tissue grafted into patients with progressing Huntington's Disease, revealing cell-to-cell transit of huntingtin aggregates *in vivo* [13]. We have previously shown that CSPα—but not the loss-of-function $CSP\alpha_{HPD\text{-}AAA}$ mutant—promotes cellular export of the polyglutamine expanded protein 72Q $huntingtin^{exon1}$ as well as mutant superoxide dismutase-1 ($SOD\text{-}1^{G93A}$) suggesting the CSPα-EV export pathway is a general pathway for the secretion of misfolded proteins [15]. Extracellular vesicles (EVs) are known to serve as mediators for the intercellular delivery of a wide array of diverse cargo to recipient cells and this heterogeneity of EVs raises the question, which EVs comprise the CSPα-EV export pathway?

In order to address this question, we first characterized total EVs released from CAD neurons. The size distribution of CAD cell EVs is shown by transmission electron microscopy (Figure 1 left panel). To characterize the heterogeneity of EVs by nanoscale flow cytometry and nanoparticle tracking analysis (NTA), we collected media from CAD cells expressing CSPα and GFP-72$huntingtin^{exon1}$, centrifuged at 300Xg for 5 min to remove cell debris and without further processing, evaluated EVs in the media (Figure 1A). The heterogeneity of particles in this unfractionated media is evident by nanoscale flow cytometry (Figure 1A, middle panel). The most frequent size distribution of EVs was found by NTA to be 144+/-2.7nm, somewhat larger than the 129+/-2.2nm [15] EVs purified by differential centrifugation/exoquick techniques as expected (data not shown).

We next sought to determine which EVs contain misfolded-GFP cargo. Nanoscale flow cytometry analysis reveals that resveratrol increases total EV secretion from control, vector and CSPα-expressing cells (Figure 1B). Secretion of EVs containing GFP-tagged 72Q $huntingtin^{exon1}$ is dramatically increased when cells express CSPα ($p < 0.0001$) and this CSPα-EV export of EVs containing GFP-72Q $huntingtin^{exon1}$ is significantly reduced by resveratrol ($p < 0.0001$). Comparison of the flow cytometry light scatter is shown in the right hand panel (Figure 1B). The majority of EVs released from CSPα-expressing CAD cells in the absence of resveratrol were the smaller <180nm, presumably exosome EVs (81.6%), while the 180-240nm EVs and the >240nm EVs were 17% and 1.4% respectively (Figure 1C, supplementary Figure 1). The bulk of EVs containing GFP-72Q $huntingtin^{exon1}$ fall within the 180-240nm range (71% ($p < 0.0001$)) and CSPα increased export of EVs containing GFP-72Q $huntingtin^{exon1}$ within this subpopulation by >400% ($p < 0.0001$). In the presence of CSPα, EVs containing GFP cargo account for 0.06% (<180nm), 1% (180-240nm) and 1.6% (>240nm) within their respective subpopulations.

Resveratrol significantly reduced secretion of the 180-240nm GFP labeled EV pool in a concentration-dependent manner while increasing export of total EVs (Figures 1B&C). In the presence of CSPα and 50μM resveratrol EVs containing GFP cargo account for 0.03% (<180nm), 0.53% (180-240nm) and 0.78% (>240nm) of the respective subpopulations (data not shown).

To investigate whether neurons secrete free floating GFP-tagged 72Q huntingtin^{exon1} entities, in addition to GFP-72Q huntingtin^{exon1} as EV cargo, we labeled EVs with Cell Mask Deep Red plasma membrane stain for 30 min at 37°C. We found that 95% of GFP-72Q huntingtin^{exon1} particles costain with Deep Red stain, confirming the GFP particles are membrane bound vesicles (Figure 1D and supplementary Figure 2). By comparison, control protein aggregates of anti CD38 do not demonstrate Deep Red staining (0.6%), while 80% of EVs containing the GFP-tagged membrane protein PC3 Palm-GFP costain with Deep Red. The GFP-containing 180-240nm membrane bound vesicles were detergent-sensitive (data not shown), as anticipated. Altogether, these results suggest that the CSPα-EV export pathway involves EVs primarily within the 180-240nm range and that resveratrol selectively inhibits the CSPα-EV export of GFP-tagged 72Q huntingtin^{exon1} while increasing overall EV export.

We next evaluated the deliverability of CSPα-EVs to naïve cells. When media (total) was applied to naive CAD neurons, GFP-72Q huntingtin^{exon1} cargo was delivered to recipient cells (Figure 1E). GFP cargo was observed in recipient cells as early as 1 hr after application of media and remained at 48 hours (Supplementary Figure 3). All recipient cells found to contain GFP-72Q huntingtin^{exon1} were rounded and without processes, however we observed a range of GFP signal intensity among GFP-positive cells suggesting the cells received different amounts of cargo. When media contained less EVs with GFP-72Q huntingtin^{exon1} cargo, for example media from neurons treated with 50μM resveratrol, GFP cargo was still detected in recipient cells (Figure 1E). These results indicate that the CSPα-EVs containing GFP-tagged 72Q huntingtin^{exon1} cargo are delivery competent. Considering that GFP positive EVs represent a fraction of total EVs, CSPαEV transfer of misfolded proteins to remote cells is potent.

Next, we subjected EVs to nanoscale flow cytometry and western blot. This parallel analysis shows that increases in cellular CSPα expression correlates with increases in 180-240nm EV export of GFP-72Q huntingtin^{exon1} without changes in the mean size of released EVs (Figure 2). Cell viability was evaluated after media collection, and was not influenced by CSPα expression (Figure 2D). The observation that transgenic expression of α-synuclein abolishes the lethality and neurodegeneration seen in CSPα knock out mice [7], raised the possibility that α-synuclein might also stimulate EV-export. That is, more than one mechanism may exist to package and export misfolded proteins from neurons. α-synuclein is the main component of the cytoplasmic inclusions formed in Parkinson's disease patients, and mutations in human α-synuclein or triplication of the α-synuclein gene cause Parkinson's disease [7,48]. We tested the

possibility that α-synuclein facilitated EV-release by comparing EV export of GFP-72Q huntingtin^{exon1} from cells expressing α-synuclein or CSPα. As shown in Figure 2E, western blot analysis reveals that increases in α-synuclein expression did not result in mutant huntingtin export. Our results rule out α-synuclein driven EV export as the mechanism underlying prevention of neurodegeneration in CSPα knock out mice and is consistent with the hypothesis that α-synuclein does not replace CSPα, but instead functions downstream of CSPα [7].

Influence of CSPα mutants on EV export.

We next evaluated the effect of CSPα mutations on EV genesis and export. L115R and L116Δ are human mutations that cause the lysosomal storage disease, ANCL, the CSPα$_{HPD-AAA}$ is a loss-of-function mutation that does not interact with Hsp70 ATPases [3,6,54,70]. The domain structure of CSPα and location of the CSPα$_{L115R}$, CSPα$_{\Delta116}$, and CSPα$_{HPD-AAA}$ mutations is shown in Figure 3A. We have previously shown that CSPα$_{L115R}$, CSPα$_{\Delta116}$, and CSPα$_{HPD-AAA}$, like wild type CSPα, are exported from cells, and while CSPα$_{L115R}$ and CSPα$_{\Delta116}$ promote export of GFP-72Htt^{exon1}, CSPα$_{HPD-AAA}$ does not [15]. We used nanoparticle tracking analysis (NTA) to evaluate the influence of mutant CSPα's on EV export in the absence of GFP-72Q huntingtin^{exon1}. The NTA profile of CSPα$_{HPD-AAA}$, CSPα$_{L115R}$ and CSPα$_{\Delta116}$ mutations relative to CSPα (blue line) is shown for comparison (Figure 3B). No difference in mean size (total) of EVs was observed as a result of CSPα mutations (Figure 3C). Furthermore, no difference in relative sizes (<180nm, 180-240nm, >240nm) of EVs was observed as a result of CSPα mutations (data not shown). We then applied conditioned media to naïve cells and monitored EV delivery of GFP-72Q huntingtin^{exon1}. Recipient cells that received control media from vector, CSPα$_{HPD-AAA,}$ and α-synuclein transfected cells showed low levels of GFP signal at 24hrs, likely due to endogenous mechanisms. Like CSPα-EVs, CSPα$_{L115R}$- and CSPα$_{\Delta116}$-EVs were delivery competent. GFP-72Q huntingtin^{exon1} aggregates were clearly observed in recipient cells as early as 1 hr and remained visible 24 hrs after media application (Supplementary figure 4). Again, recipient cells contained a range of GFP signal intensity suggesting the receipt of different amounts of cargo and all GFP positive cells were rounded and without processes.

How does resveratrol reduce the export of GFP- 72Q huntingtin^{exon1} by CSPα-EVs? To address this question neurons were treated with 50μM resveratrol 6 hrs following transfection. Figure 4A shows the NTA profile of EVs collected in the presence and absence of 50μM resveratrol (red Line). Resveratrol reduced secretion of GFP-72Q huntingtin^{exon1} but not CSPα (Figure 4B), consistent with earlier observations [15]. Moreover, resveratrol reduced secretion of GFP-72Q huntingtin^{exon1} mediated by CSPα, CSPα$_{L115R}$ and CSPα$_{\Delta116}$. Cell viability following media removal is shown in the right hand panel. Nanoscale flow cytometry analysis verified that resveratrol increased total EVs exported by CAD cells in all conditions, while decreasing GFP-72Q huntingtin^{exon1}-containing EVs. Resveratrol also significantly, increased the mean size

of vesicles in all conditions (Figure 4C). One possibility is that resveratrol may directly influence cargo-loading machinery of the CSPα EVs. It is also conseivable that resveratrol might indirectly influence cargo-loading by modulating other proteostatic mechanisms that target GFP-72Q huntingtin^{exon1} (eg proteasome, lysosome clearance). Taken together, these results indicate that resveratrol reduces cargo-loading of GFP-tagged 72Q huntingtin^{exon1} into EVs without reducing export of CSPα or the CSPα$_{L115R}$ and CSPα$_{\Delta116}$.

DnaJB2 and DnaJB6-EV Export Pathways.

CSPα (DnaJC5) is a type III J Protein with a well-defined domain architecture that includes an N terminal J domain and a cysteine string region after which the protein is named [5]. J proteins are a family of chaperones that contain a wide variety of domains but the defining signature domain is the ~70 amino acid J domain that contains a histidine-proline-aspartic acid (HPD) motif required for activation of Hsp70 [40]. This led to the speculation that other J proteins may also export misfolded proteins.

In order to test this prediction we screened several J proteins with reported links to neurodegeneration [75] for EV-export activity. DnaJB2 was identified by both western analysis (left panel) and nanoscale flow cytometry (right panel) as a J protein that exports misfolded huntingtin in EVs similar to CSPα (Figure 5A&B). Alternative splicing of the DnaJB2 gene produces two isoforms, a DnaJB2$_{short}$ and a 42kDa DnaJB2$_{long}$ isoform [10] that undergoes C terminal geranylgeranylation [8], we studied DnaJB2$_{long}$. The related J proteins, DnaJA1, DnaJB1, DnaJB11, DnaJC14, DnaJC13 and DnaJC19 did not export misfolded huntingtin. Extracellular milieu includes free floating co-chaperones in addition to EVs, and chaperones that adhere to EVs were expected to co-isolate with EVs. We found that DnaJA1, DnaJB1, DnaJB2, DnaJB6, DnaJB11 and DnaJC14 were secreted from CAD cells (Figure 5C). In fact, DnaJB11 as well as DnaJA1 were robustly secreted by CAD neurons under all conditions evaluated (Figure 5C). DnaJB11(Erdj3) is known to be secreted via the conventional secretory pathway [24], on the other hand DnaJB1 is secreted in exosomes [68] and the mechanisms underlying DnaJA1 and DnaJC14 secretion remain to be determined. Whether or not secreted J proteins activate Hsp70 ATPase for conformational work would depend on ATP levels and remains to be fully elucidated.

A confounding observation from the parallel analysis was that DnaJB6$_{short}$ was observed to export GFP-72Q huntingtin^{exon1} by nanoscale flow cytometry but not western analysis (Figure 5A). This suggested to us that cargo in DnaJB6 EVs may undergo degradation during EV isolation. To investigate further we analyzed GFP-72Q huntingtin^{exon1} export by spotting media on nitrocellulose prior to EV purification. Dot blot analysis of unfractionated media (data not shown) and western blot of EVs (Figure 6A), reveal that at high expression levels DnaJB6$_{short}$ did indeed mediate export of GFP-72Q huntingtin^{exon1}. Alternative splicing of the DnaJB6 gene produces two isoforms, a DnaJB$_{short}$ and a 36kDa DnaJB6$_{long}$ isoform that contains a C terminal

nuclear localization signal [51]. We compared $DnaJB6_{short}$ and $DnaJB6_{long}$ for GFP-72Q huntingtin^{exon1} export activity. To our surprise, EV export of GFP-72Q huntingtin^{exon1} by $DnaJB6_{long}$ was more robust than $DnaJB6_{short}$ by western analysis. Domain structures of CSPα, $DnaJB2_{long}$ and $DnaJB6_{long}$ are shown in Figure 6B. Each of these co-chaperones contains unique domains in addition to the common J domain. Figure 6C shows the percentage of GFP positive EVs within the total pool determined by nanoscale flow cytometry (left panel) and quantification of GFP-72Q huntingtin^{exon1} by western analysis (right panel). The percent of EVs containing GFP-72Q huntingtin^{exon1} is dramatically increased when cells express CSPα ($p < 0.0001$), $DnaJB2_{long}$ ($p < 0.0001$) or $DnaJB6_{long}$ ($p < 0.0001$). EVs containing GFP-72Q huntingtin^{exon1} are primarily within the 180-240nm range from $DnaJB2_{long}$ and $DnaJB6_{long}$ expressing cells, similar to that found for cells expressing CSPα. We found that exported $DnaJB2_{long}$- and $DnaJB6_{long}$-EVs containing GFP-72Q huntingtin^{exon1} deliver cargo to recipient cells (supplementary figure 5). In contrast to CSPα and CSPα mutants, media containing $DnaJB2_{long}$ and $DnaJB6_{long}$ EVs did not deliver GFP-huntingtin^{exon1} to recipient cells at 1 hr but were observed to deliver cargo 24 hrs following media application. These results indicate that while $DnaJB2_{long}$ and $DnaJB6_{long}$ EVs transfer GFP-72Q huntingtin^{exon1} between cells there are differences in recipient cell uptake or proteostasis between $DnaJB2_{long}$/$DnaJB6_{long}$ and CSPα EVs.

Collectively our results show that three J proteins that are key to neuronal protein quality control, CSPα, $DnaJB2_{long}$, $DnaJB6_{long}$ shuttle misfolded GFP-72Q huntingtin^{exon1} from parent to recipient cells in EVs and that the molecule resveratrol modulates this pathway. These removal-based mechanisms represent >1% of the total EVs produced, and yet, efficiently transfer neurotoxic components to naïve cells.

Discussion

Here we report that the J proteins, CSPα (DnaJC5), DnaJB2$_{long}$ and DnaJB6$_{long}$ promote export of misfolded 72Q huntingtin^{exon1} in extracellular vesicles (EVs). Successful intercellular transmission is achieved via these EVs. We found that GFP-72Q huntingtin^{exon1} is primarily located in EVs within the 180-240nm size range. Intervention in these J protein removal based mechanisms is promising, given that resveratrol, a common dietary component, strongly inhibits 72Q huntingtin^{exon1} transport through the CSPα-EV export pathway. J Protein co-chaperones orchestrate a number of diverse intracellular proteostasis functions, our data provides a clear role for CSPα (DnaJC5), DnaJB2$_{long}$ and DnaJB6$_{long}$ in facilitating misfolded protein export. Earlier work demonstrated that CSPα increases secretion of TDP-43, α-synuclein and tau from HEK293 cells [22] and exports SOD-1^{G93A} and 72Q huntingtin^{exon1} in EVs [15] suggesting that several disease-causing proteins transit through this pathway.

The proteostasis network consists of elaborate and incredibly adaptive protein machinery that protects against age-associated neuronal decline and neurodegenerative disorders [52]. The role of CSPα, DnaJB2 and DnaJB6 in neural quality control mechanisms are supported by genetic as well as experimental evidence. Human mutations in CSPα (DnaJC5) and DnaJB6 lead to adult neuronal ceroid lipofuscinosis (ANCL) [3,54,70], and limb-girdle muscular dystrophy [33,57,62,63,67] respectively. Mutations in DnaJB2, depending on their location, cause Charcot Marie Tooth disease type 2 [25], distal hereditary motor neuropathy [4], spinal muscular atrophy or juvenile Parkinsonism [61]. The association of DnaJB2 with neurofibrillary tangles in Alzheimer's disease patients [10], the presence of DnaJB6 in lewy bodies in Parkinson's disease patients [17] and the intralysosomal accumulation of lipofuscin caused by CSPα mutations [3,54,70] link these J proteins to neural quality control mechanisms. In addition, DnaJB2 overexpression reduces huntingtin and SOD-1 aggregation in mouse models of Huntington's disease and amyotrophic lateral sclerosis [35,45,55]. In *drosophila* and *xenopus*, overexpression of DnaJB6 suppresses polyglutamine toxicity [19,32] and, in mice, brain-specific overexpression of DnaJB6 delays polyglutamine aggregation and onset of disease [37]. In the absence of DnaJB6, mice die mid-gestation due to a failure of chorioallantoic attachment during placental development and keratin aggregation [73]. Moreover, the absence of CSPα leads to neurodegeneration in *drosophila*, mice and *c. elegans* [20,41,77]. *In vitro,* DnaJB6 inhibits Aβ amyloid aggregation [47]. In cellular models, DnaJB6 suppresses huntingtin, ataxin-3 and androgen receptor aggregation [12,26,32], while the absence of DnaJB6 leads to α-synuclein aggregation [2] and DnaJB2 suppresses rhodopsin, huntingtin, ataxin-3, parkin and TDP-43 aggregation [8,11,23,60,74]. Considering the conserved nature of EV shuttles, alongside the CSPα, DnaJB2 and DnaJB6 links to quality control, the data in this report expands our understanding of proteostasis to include J protein-driven EV transfer of disease-causing misfolded proteins. The newly-identified J protein-EV pathways by which neurons transfer neurotoxic proteins to cells have similarities to tunneling nanotube and exofer (4μm) systems that also transport polyglutamine expanded huntingtin [14,49].

Perhaps the most unexpected observation in this report is that DnaJB6$_{long}$, which contains a nuclear localization signal (NLS) [51], exports misfolded GFP-72Q huntingtin^{exon1} in EVs. The cellular machinery that targets proteins, or more specifically misfolded/aggregated proteins, into EVs is not fully elucidated. Plasma membrane anchors are proposed to be involved in EV protein packaging pathways [65]. CSPα is one of the most heavily palmitoylated

proteins known [56] and DnaJB2$_{long}$ undergoes geranylgeranylation [8]. Interestingly, DnaJB2$_{long}$ contains two unique ubiquitin interacting motifs that bind ubiquitylated proteins and target them for clearance [9]. We do not know why CSPα, DnaJB2$_{long}$ and DnaJB6$_{long}$ sort GFP-72Q huntingtin^{exon1} to EVs and the other J proteins failed to do so. Clearly, the common J domain is not the only molecular determinant for EV-export of misfolded 72Q huntingtin^{exon1} and the specific domains that mediate cargo selectivity of these pathways requires future studies. It is conceivable that the distinct domains of these three J proteins allows for greater level of adaptability in the recruitment of misfolded clients for export. Such molecular characterization of chaperone activity in EVs will undoubtedly be the focus of future experimentation.

Neural export of misfolded proteins offers many advantages. The capacity of EVs to transfer misfolded/aggregated protein cargo like GFP-72Q huntingtin will influence proteostasis of both recipient and parent cells. The export of misfolded proteins could relieve pressure on parent cell proteostasis machinery and deliver misfolded proteins to cells with greater folding/clearance capacity. This would be particularly relevant in neurons where, for example, synapse-specific proteostasis is almost certainly limited, and yet, proteins susceptible to misfolding and aggregation are abundant [28]. EV export would greatly improve clearance of toxic proteins that synapses are unable to digest. The strategy to save resources by exporting unfolded and aggregated proteins in EVs for offsite degradation pathways predicts that EVs containing misfolded cargo would be specifically targeted to cells equipped to process toxic protein aggregates. Little is known about the signals that target EVs to recipient cells and the mechanisms underlying uptake differences in EVs that remove unwanted proteins vs EVs that pathologically spread disease-causing proteins. Although, it is widely agreed that in neurodegenerative disorders, there is a relationship between EVs and the spread of misfolded-disease-causing proteins including prions, amyloid peptides, α-synuclein, SOD-1, TDP-43, and tau [1,15,18,21,27,29,30,53,58,59,64,66,71]. The ultimate question of how CSPα (DnaJC5), DnaJB2$_{long}$ and DnaJB6$_{long}$ EVs function in neurodegenerative disease progression remains to be determined.

To our knowledge, our results illustrate the first examples of J protein co-chaperones that transfer misfolded proteins between cells, enabling clearance of neurotoxic proteins from parent cells and delivery to recipient cells. Our study suggests a mechanism for how neurons restore proteostasis and suggest that dysregulation of this pathway may contribute to pathogenic disease progression in neurodegenerative disorders, although the significance of J protein mediated EV export *in vivo* is far from clear.

Figures

Figure 1. Resveratrol reduces export of GFP-72Htt^{exon1} cargo by CSPα-EVs. (A) Transmission electron microscopy (left panel) and nanoscale flow cytometry analysis (middle panel) of total EVs secreted from CAD cells expressing CSPα and GFP-72Htt^{exon1}. Illustration showing the experimental approach to probe total EVs (right panel). (B) Bar graphs (left panels) and nanoscale flow cytometry scatter plot (right panel) show the concentration of total and GFP-72Htt^{exon1} containing EVs in the presence and absence of 50μM resveratrol. (C) Graphs (left panels) and flow cytometry scatter plot (right panel) showing the resveratrol concentration response on total and GFP-72Htt^{exon1} containing EVs levels. (D) GFP-72Htt^{exon1} containing EVs costain with Deep Red membrane stain. (E) Representative images of GFP fluorescence of recipient cells. Unfractionated media collected from CAD cells expressing GFP- 72Q Htt^{exon1} and CSPα in the absence (top panels) and presence (bottom panels) of 50μM resveratrol was applied to naïve CAD cells. Two hours following media application live cells were imaged. The experiment was replicated ten-twelve times (**P<0.01, ****P<0.0001)

Figure 2. Export of EVs carrying 72Q Htt^{exon1} by CSPα is concentration dependent. Nanoscale flow cytometry analysis showing (A) GFP-72Q Htt^{exon1}–containing and total (B) EV concentration collected from CAD neurons expressing different levels of CSPα. (C) Mean size of total EVs. (D) Relative cell viability of CAD cells following media collection. (E) Western analysis of EVs collected from CAD cells expressing GFP-tagged 72Q Htt^{exon1} and CSPα or α-synuclein. Blots are probed for GFP and flotillin. Western blot is representative of 4 independent experiments. Flotillin is shown as a loading control. (*P<0.05, **P<0.01, ***P<0.001, ****P<0.0001)

Figure 3. Influence of CSPα mutants on EV export. (A) Domain structure of CSPα highlighting the CSPα$_{HPD-AAA,}$ CSPα$_{L115R}$ and CSPα$_{\Delta 116}$ mutations. (B) NTA analysis of total EVs exported from CAD cells expressing CSPα mutants (but not GFP-72Htt^{exon1}); Mean histogram data for CSPα is overlaid in blue for comparison. (C) Mean size of total EVs exported from CAD cells.

Figure 4. Resveratrol reduces export of GFP-72Htt^{exon1} cargo by CSPα. (A) NTA analysis of total EVs exported from CAD cells expressing the indicated CSPα mutants and GFP-72Htt^{exon1}. (B) Western analysis (left panel) of EVs collected from CAD cells expressing the indicated CSPα mutants in the presence (+) and absence (-) of 50μM resveratrol. Western blots are probed for GFP, flotillin and CSPα. Relative cell viability (right panel) of CAD cells post media collection. (C) Concentration of GFP-72Htt^{exon1}–containing EVs (left panel), and mean size (middle panel) and concentration of total EVs (right panel) was determined by nanoscale flow cytometry. (*P<0.05, **P<0.01, ***P<0.001, ****P<0.0001)

Figure 5. DnaJB2 and DnaJB6 promote EV export of 72Q huntingtin^{exon1}. (A) Quantification by western analysis (left panel) and nanoscale flow cytometry (right panel) of secreted GFP-tagged 72Q huntingtin^{exon1} from cells expressing GFP-tagged 72Q huntingtin^{exon1} and vector, myc-

tagged CSPα, CSPα$_{HPD-AAA}$, DnaJA1, DnaJB1, DnaJB2$_{long}$, DnaJB6$_{short}$, DnaJB11, DnaJC13, DnaJC14, DnaJC19 and α-synuclein. (B) Representative immunoblot of EV's collected from cells expressing the indicated proteins. Blot is probed for GFP and flotillin. Flotillin is shown as a loading control. (C) Western analysis of EVs collected from CAD cells expressing the indicated proteins. Western blots are probed for the proteins indicated on the right. ****P<0.0001

Figure 6. EV export of 72Q huntingtin^{exon1} by DnaJB2$_{long}$ and DnaJB6$_{long}$. (A) Western blot analysis of EVs from neurons expressing DnaJB6 isoforms probed with anti-huntingtin and anti-GFP (right panel). Western analysis of EVs collected from CAD cells transfected with 3.5μg GFP-tagged 72Q Htt^{exon1} and 3.5μg vector, 3.5μg CSPα, 3.5 and 4.5μg DnaJB2$_{long}$, 3.5 and 4.5μg of DnaJB6$_{long}$ and 3.5 and 4.5μg of DnaJB6$_{short}$ probed with anti-GFP. (B) Domain structure of CSPα, DnaJB2$_{long}$ and DnaJB6$_{long}$ highlighting the common J domains and unique cysteine string region (CCC), ubiquitin interacting motifs (UIM), CAAX box and Nuclear localization signal (NLS). (C) Percentage of GFP positive in the total EV pool determined by nanoscale flow cytometry Left panel) and Quantification of secreted GFP-tagged 72Q huntingtin^{exon1}. (*P<0.05, **P<0.01, ***P<0.001, ****P<0.0001).

Supplementary Figures

Figure S1. (A) Scatter of nanoscale flow cytometry size standards including both fluorescent latex and non-fluorescent silica standards ranging in size from 110nm – 1300nm. (B) Red lines illustrate the division of size ranges of detected EVs described in the text to carry GFP-tagged 72Q Htt^{exon1} cargo. (C) NTA size standards (mean) included 60nm, 200nm and 400nm polystyrene NIST size standards as well as a 100nm silica size standards.

Figure S2. (A) NTA analysis of anti-CD36FITC antibody aggregation. (B) Line graph of the time dependent aggregation of anti-CD36-PE antibody (C) NTA profiles of anti-CD36-FITC (orPE) antibody aggregation.

Figure S3. (Top panel) GFP-72Htt^{exon1} aggregates in donor CAD cells at the time of media collection. (Lower panels) GFP-72Htt^{exon1} aggregates in recipient CAD cells. Time after media application is indicated. white scale bar = 200μm; orange scale bar = 50μm.

Figure S4. Representative images of GFP-72Htt^{exon1} aggregates in donor cells transfected with DNA encoding 3.5μg CSPα, CSPα$_{L115R}$, CSPα$_{Δ116}$, CSPα$_{HPD-AAA}$ or 4.5ug of α-synuclein. Recipient CAD cells are shown 1 hr and 24hrs after application of conditioned media. white scale bar = 200μm; orange scale bar = 50μm

Figure S5. Representative images of GFP-72Htt^{exon1} aggregates in recipient CAD cells 1 hr and 24hrs after application of conditioned media from cells transfected with DNA encoding 3.5μg CSPα, 4.5μg DnaJB2$_{long-}$, 4.5μg and 4.5μg DnaJB6$_{long}$. White scale bar = 200μm; orange scale bar = 50μm.

Materials and Methods

EV collection from CAD cells

Maintenance of CAD (catecholaminergic derived CNS cells) was described before [15,44]. For expression in CAD cells, cDNAs encoding for Myc-tagged J proteins and GFP-72Q huntingtin^{exon1} were transiently transfected with Lipofectamine 3000 (Invitrogen) in Opti-MEM™ medium. Media was changed to serum-free media 6 hrs post-transfection, and, resveratrol treatment began at the media change. Media was collected 48 hrs after transfection, spun at 300Xg for 5 min to remove cell debris and evaluated without further processing by nanocyte tracking analysis, nanoscale flow cytometry analysis and dot blot analysis. For western analysis EVs were isolated from the unfractionated media by exoquick precipitation solution (SBI) and solubilized in sample buffer. Following media collection, cell viability was determined utilizing an XTT assay (New England Biolabs).

Immunoblotting

Proteins were separated by SDS-PAGE and electrotransferred from polyacrylamide gels to nitrocellulose membrane (0.2µm pore size). Membranes were blocked in tris-buffered saline (TBS) containing 0.1 % Tween 20, 1 % BSA and then incubated with primary antibody overnight at 4°C. The membranes were washed and incubated with horseradish peroxidase-coupled secondary antibody for ~2 hrs at room temperature. Bound antibodies on the membranes were detected by incubation with Pierce chemiluminescent reagent and exposure to Cdigit, LiCor (Mandel). The chemiluminescent signals were quantified using image studio digits software (Mandel). For the dot blots, 10µl of unfractionated media was spotted on nitrocellulose membrane, dried and membrane processed as described above.

Plasmids

cDNAs encoding for CSPα, CSPα mutants, and J proteins were expressed in the plasmid myc-pCMV. GFP-72Q huntingtin^{exon1} was expressed in the plasmid pcDNA3.1. All amplified regions of all plasmids were sequenced to ensure the absence of any undesired mutations.

Transmission Electron Microscopy

Media was centrifuged at 2,000g for 10 min, and at 10,000Xg for 30 min to discard membrane and debris. The supernatant was then centrifuged at 100,000g for 2 hrs and EVs collected. EVs were suspended in PBS, fixed sequentially on a 150 mesh grid in 4% paraformaldehyde followed by 2% glutaraldehyde and stained with 2% uranyl acetate for 10 min. EVs were imaged with a Tecnai F20 TEM and a Gaten CCD camera.

Fluorescence Imaging

Images of live cells were taken with the EVOS FL Auto Imaging System. Images of donor cells were taken at the time of media collection. Images of recipient cells were taken between 1-48 hours. The intensity of the GFP-72Q Htt^{exon1} varied among cells and we used the single slider until the on-screen brightness of the lowest intensity aggregate was satisfactory and used this setting to capture images in high-quality mode.

Nanoparticle Tracking Analysis

For NTA and nanoscale flow cytometry analysis, all samples were diluted 25 fold using 0.2x phosphate buffered saline that had been filtered twice through 0.2micron filter. For NTA analysis, all samples were analyzed using the Nanosight LM10 (405nm laser, 60mW, software version 3.00064). Samples were analyzed in triplicate for 60 seconds per replicate with a count range of 20-100 particles per frame. A variety of NIST (Thermo Scientific 3000 Series) standards (Supplementary Materials) were analyzed each today prior to sample analysis. The system was cleaned between each sample and checked for any sample carryover using the PBS diluent.

Nanoscale Flow Cytometry

Samples were similarly prepared for nanoscale flow cytometry as for NTA. All samples were analyzed using the Apogee A50 flow cytometry platform. Light scatter was provided using the 405nm laser (75mW); GFP signal was generated using the 488nm laser (50mW, 535/35) and far red signal was generated using the 630nm laser (75mW, 680/35). All samples were analyzed for 60 seconds. Optimization was performed to insure single EVs were being analyzed and single events were triggered by light scatter only. The system was cleaned each day prior to sample analysis and a variety of silica and polystyrene standards (Apogee 1493 standards) processed for instrument set up and QC. The silica standards were used to assess the relative size range of EVs (see supplementary Figure 1).

To demonstrate that the GFP-72Q Htt^{exon1} signal was associated with bona fide vesicles and not simply protein aggregates, samples were first mixed with Cell Mask Deep Red plasma membrane stain (Thermo Fisher Scientific (C10046), final concentration of 0.1X), incubated for 30 minutes at 37°C and then diluted in PBS. Palmitoylated-GFP positive EVs were obtained from the conditioned media of a PC3 prostrate cancer cell line; the membrane of these EVs contains the FP proteins. Anti-CD-FITC antibody was used to generate protein aggregates. Antibody (10µl) aliquots were incubated at 50°C for increasing periods of time to generate non-membrane, protein aggregates. These aggregates as well as the PC PALM-GFP controls were similarly stained with Deep Red cell mask. Aggregate concentration was analyzed by NTA and uptake of the membrane dye was measured using nanoscale flow cytometry. For these experiments, single particle detection was triggered using positive GFP/FITC fluorescence and the associated far red signal analyzed.

Statistical Analysis

All data were graphed and statistically analyzed using GraphPad Prism version 6.01 for Windows, GraphPad Software, La Jolla California USA, www.graphpad.com. Statistics included One-Way and Two Way ANOVA with either Tukey's or Dunnett's post test analysis if initial ANOVA was statistically significant ($p<0.05$; stars indicate significance ★ $p<0.05$, ★★ $p<0.01$, ★★★ $p<0.001$, ★★★★ $p<0.0001$). All values are presented as the mean ±SEM where appropriate, otherwise the SD is presented as indicated.

Acknowledgements
The work was supported by a grant from the Alzheimer Society of Alberta and Northwest Territories, the Alberta Prion Research Institute and National Research Council of Canada. The authors would like to express their gratitude to Dr. Frank Visser for technical support and Ali Jalloul for technical advice.

Author Contributions
J.E.A.B. conceived the project. D.P. and J.L. designed and interpreted all NTA and NFC experiments. J.E.A.B designed and interpreted all WB and FI experiments. J.D. provided technical assistance. J.E.A.B. D.P. and J.L. wrote the manuscript.

The authors declare they have no competing financial interests.

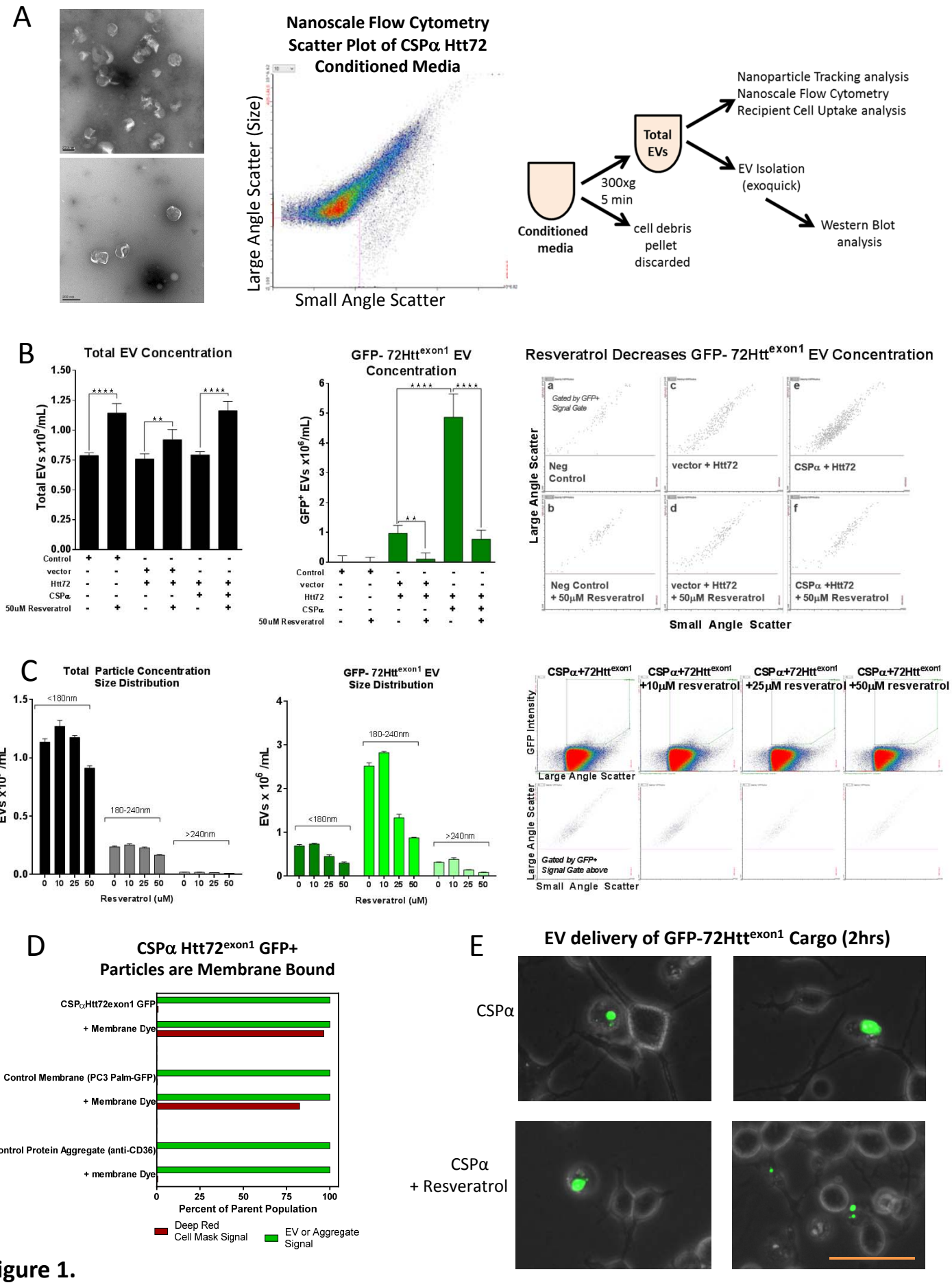
A
Nanoscale Flow Cytometry
Scatter Plot of CSPα Htt72
Conditioned Media
Large Angle Scatter (Size)
Small Angle Scatter
Conditioned media
300xg
5 min
cell debris
pellet
discarded
Total
EVs
Nanoparticle Tracking analysis
Nanoscale Flow Cytometry
Recipient Cell Uptake analysis
EV Isolation
(exoquick)
Western Blot
analysis
B
Total EV Concentration
Total EVs x10^9/mL)
Control
vector
Htt72
CSPα
50uM Resveratrol
GFP- 72Htt^exon1 EV
Concentration
GFP+ EVs x10^6/mL)
Resveratrol Decreases GFP- 72Htt^exon1 EV Concentration
Gated by GFP+
Signal Gate
Neg
Control
vector + Htt72
CSPα + Htt72
Neg Control
+ 50μM Resveratrol
vector + Htt72
+ 50μM Resveratrol
CSPα +Htt72
+ 50μM Resveratrol
Large Angle Scatter
Small Angle Scatter
C
Total Particle Concentration
Size Distribution
EVs x10^9 /mL
<180nm
180-240nm
>240nm
Resveratrol (uM)
GFP- 72Htt^exon1 EV
Size Distribution
EVs x 10^6 /mL
CSPα+72Htt^exon1
CSPα+72Htt^exon1
+10μM resveratrol
CSPα+72Htt^exon1
+25μM resveratrol
CSPα+72Htt^exon1
+50μM resveratrol
GFP Intensity
Large Angle Scatter
Gated by GFP+
Signal Gate above
Small Angle Scatter
D
CSPα Htt72^exon1 GFP+
Particles are Membrane Bound
CSPαHtt72exon1 GFP
+ Membrane Dye
Control Membrane (PC3 Palm-GFP)
+ Membrane Dye
Control Protein Aggregate (anti-CD36)
+ membrane Dye
Percent of Parent Population
Deep Red
Cell Mask Signal
EV or Aggregate
Signal
E
EV delivery of GFP-72Htt^exon1 Cargo (2hrs)
CSPα
CSPα
+ Resveratrol

Figure 1.

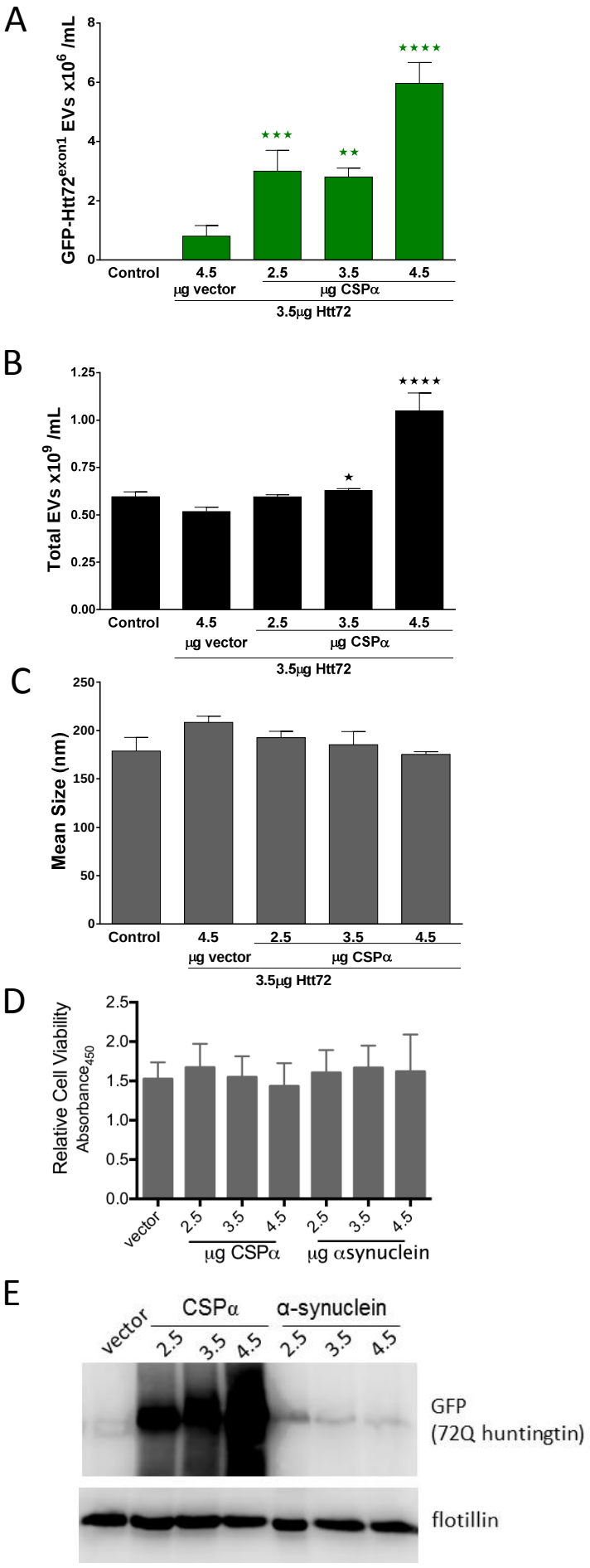
A
GFP-Htt72exon1 EVs x10^6 /mL
Control
4.5
2.5
3.5
4.5
µg vector
µg CSPα
3.5µg Htt72
B
Total EVs x10^9 /mL
Control
4.5
2.5
3.5
4.5
µg vector
µg CSPα
3.5µg Htt72
C
Mean Size (nm)
Control
4.5
2.5
3.5
4.5
µg vector
µg CSPα
3.5µg Htt72
D
Relative Cell Viability
Absorbance450
vector
2.5
3.5
4.5
2.5
3.5
4.5
µg CSPα
µg αsynuclein
E
vector
CSPα
α-synuclein
2.5
3.5
4.5
2.5
3.5
4.5
GFP
(72Q huntingtin)
flotillin

Figure 2.

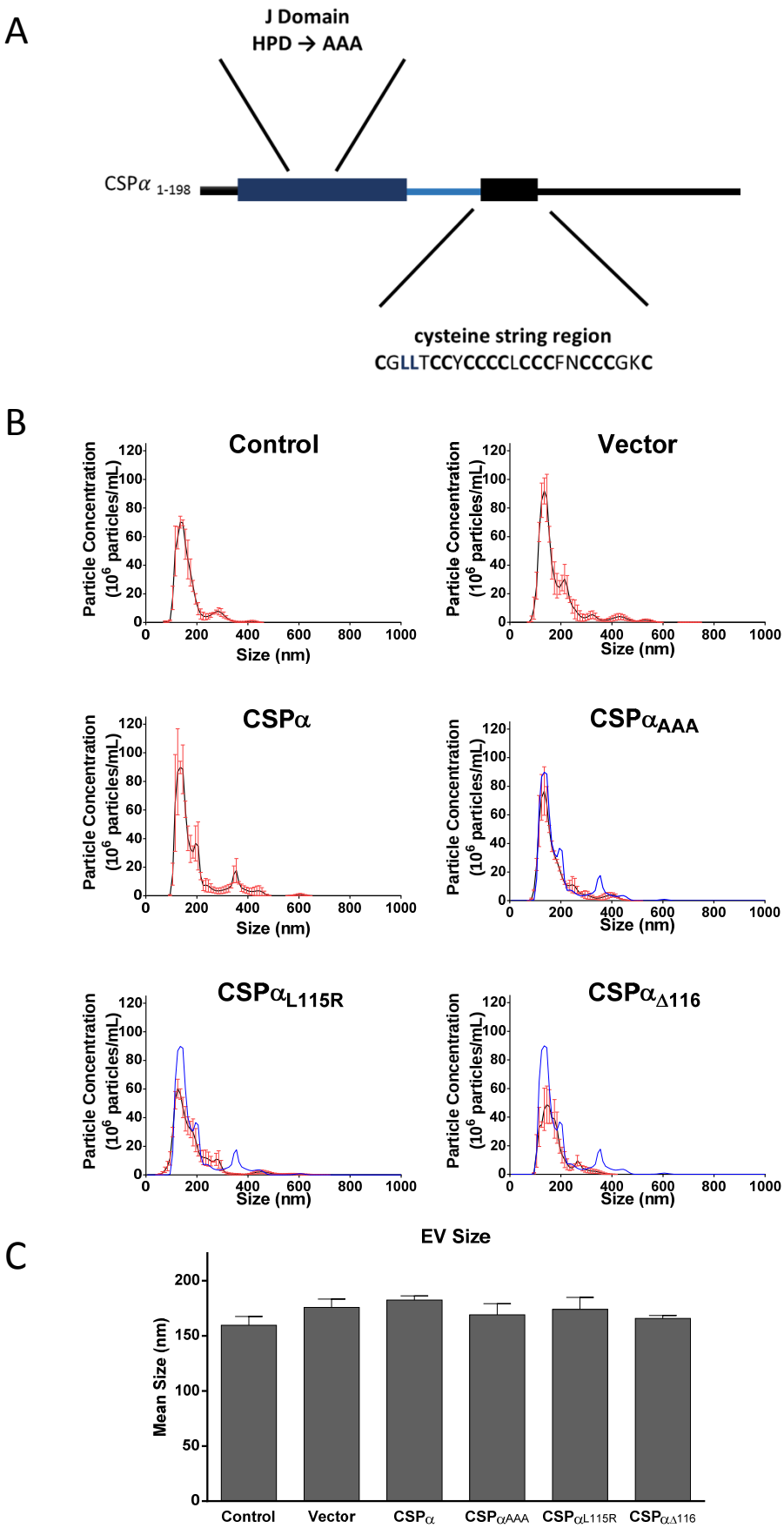
A
J Domain
HPD → AAA
CSPα 1-198
cysteine string region
CGLLTCCYCCCCLCCCFNCCCGKC
B
Control
Vector
CSPα
CSPαAAA
CSPαL115R
CSPαΔ116
Particle Concentration (10^6 particles/mL)
Size (nm)
C
EV Size
Mean Size (nm)
Control
Vector
CSPα
CSPαAAA
CSPαL115R
CSPαΔ116

Figure 3.

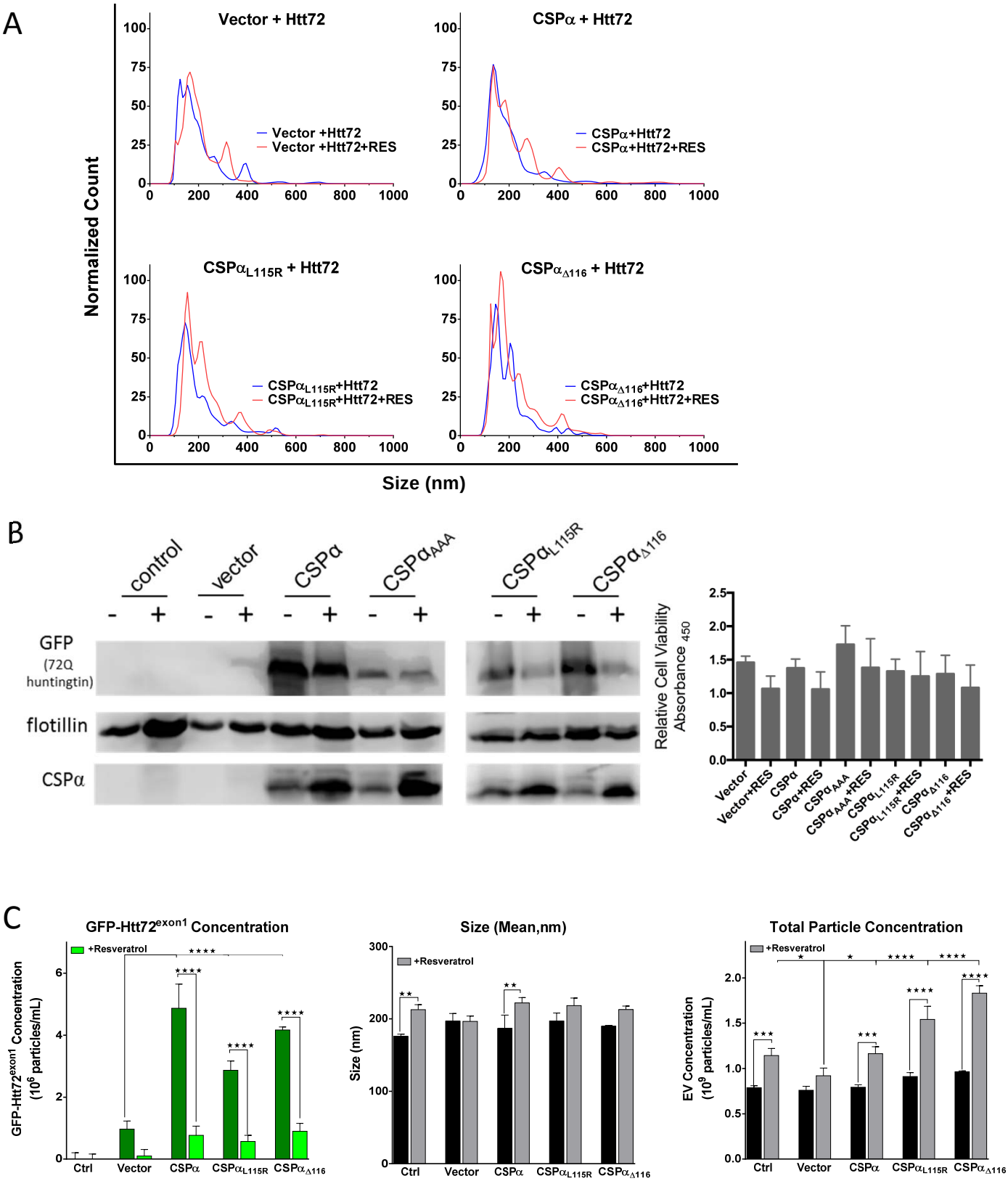
A
Vector + Htt72
CSPα + Htt72
CSPα$_{L115R}$ + Htt72
CSPα$_{Δ116}$ + Htt72
Vector +Htt72
Vector +Htt72+RES
CSPα+Htt72
CSPα+Htt72+RES
CSPα$_{L115R}$+Htt72
CSPα$_{L115R}$+Htt72+RES
CSPα$_{Δ116}$+Htt72
CSPα$_{Δ116}$+Htt72+RES
Normalized Count
Size (nm)
B
control
vector
CSPα
CSPα$_{AAA}$
CSPα$_{L115R}$
CSPα$_{Δ116}$
GFP
(72Q huntingtin)
flotillin
CSPα
Relative Cell Viability
Absorbance 450
Vector
Vector+RES
CSPα
CSPα+RES
CSPα$_{AAA}$
CSPα$_{AAA}$+RES
CSPα$_{L115R}$
CSPα$_{L115R}$+RES
CSPα$_{Δ116}$
CSPα$_{Δ116}$+RES
C
GFP-Htt72^{exon1} Concentration
+Resveratrol
GFP-Htt72^{exon1} Concentration (10^6 particles/mL)
Size (Mean,nm)
Size (nm)
Total Particle Concentration
EV Concentration (10^9 particles/mL)
Ctrl
Vector
CSPα
CSPα$_{L115R}$
CSPα$_{Δ116}$

Figure 4.

A

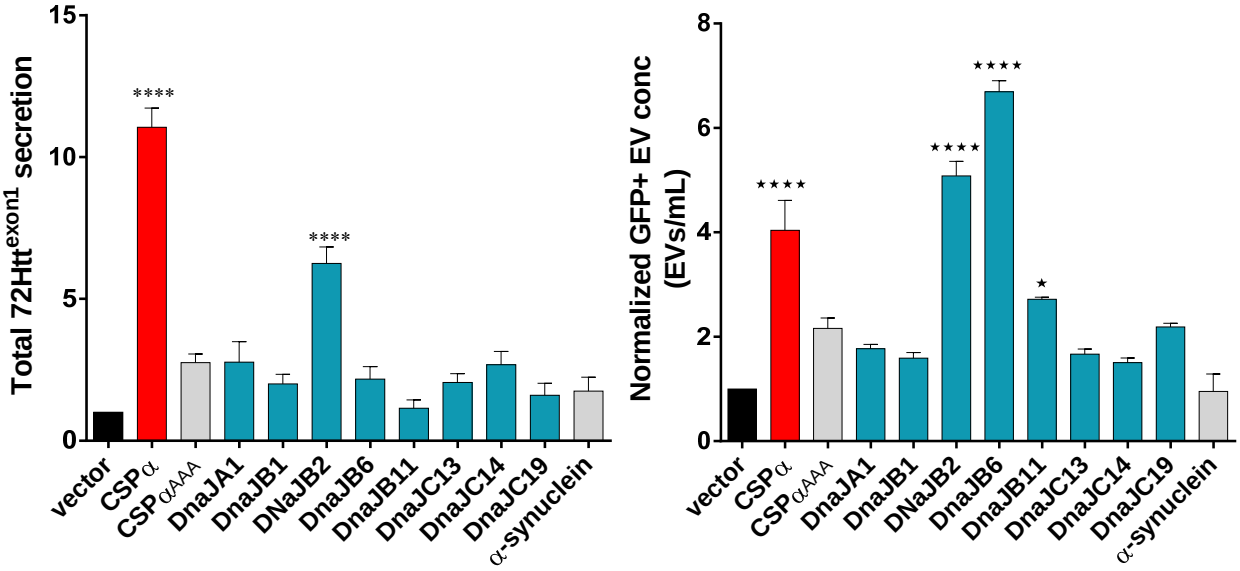
Total 72Htt exon1 secretion
15
10
5
0
****
****
vector
CSPα
CSPαAAA
DnaJA1
DnaJB1
DNaJB2
DnaJB6
DnaJB11
DnaJC13
DnaJC14
DnaJC19
α-synuclein
Normalized GFP+ EV conc (EVs/mL)
8
6
4
2
0
****
****
****
*

B

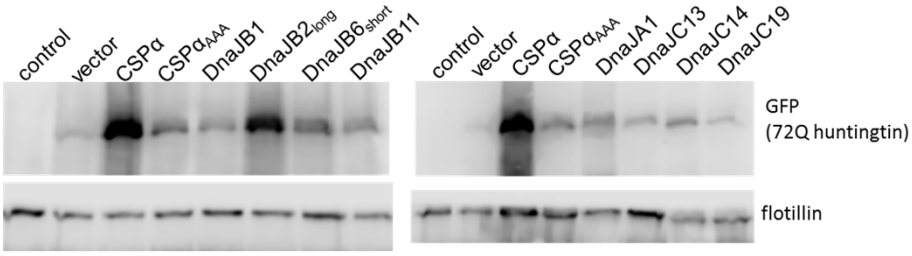
control
vector
CSPα
CSPαAAA
DnaJB1
DnaJB2long
DnaJB6short
DnaJB11
control
vector
CSPα
CSPαAAA
DnaJA1
DnaJC13
DnaJC14
DnaJC19
GFP
(72Q huntingtin)
flotillin

C

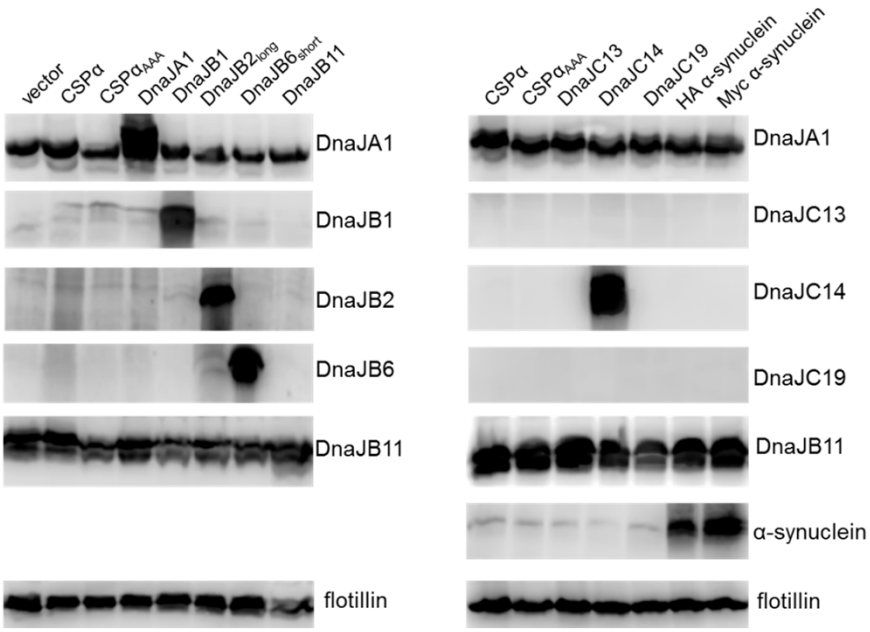
vector
CSPα
CSPαAAA
DnaJA1
DnaJB1
DnaJB2long
DnaJB6short
DnaJB11
DnaJA1
DnaJB1
DnaJB2
DnaJB6
DnaJB11
flotillin
CSPα
CSPαAAA
DnaJC13
DnaJC14
DnaJC19
HA α-synuclein
Myc α-synuclein
DnaJA1
DnaJC13
DnaJC14
DnaJC19
DnaJB11
α-synuclein
flotillin

Figure 5.

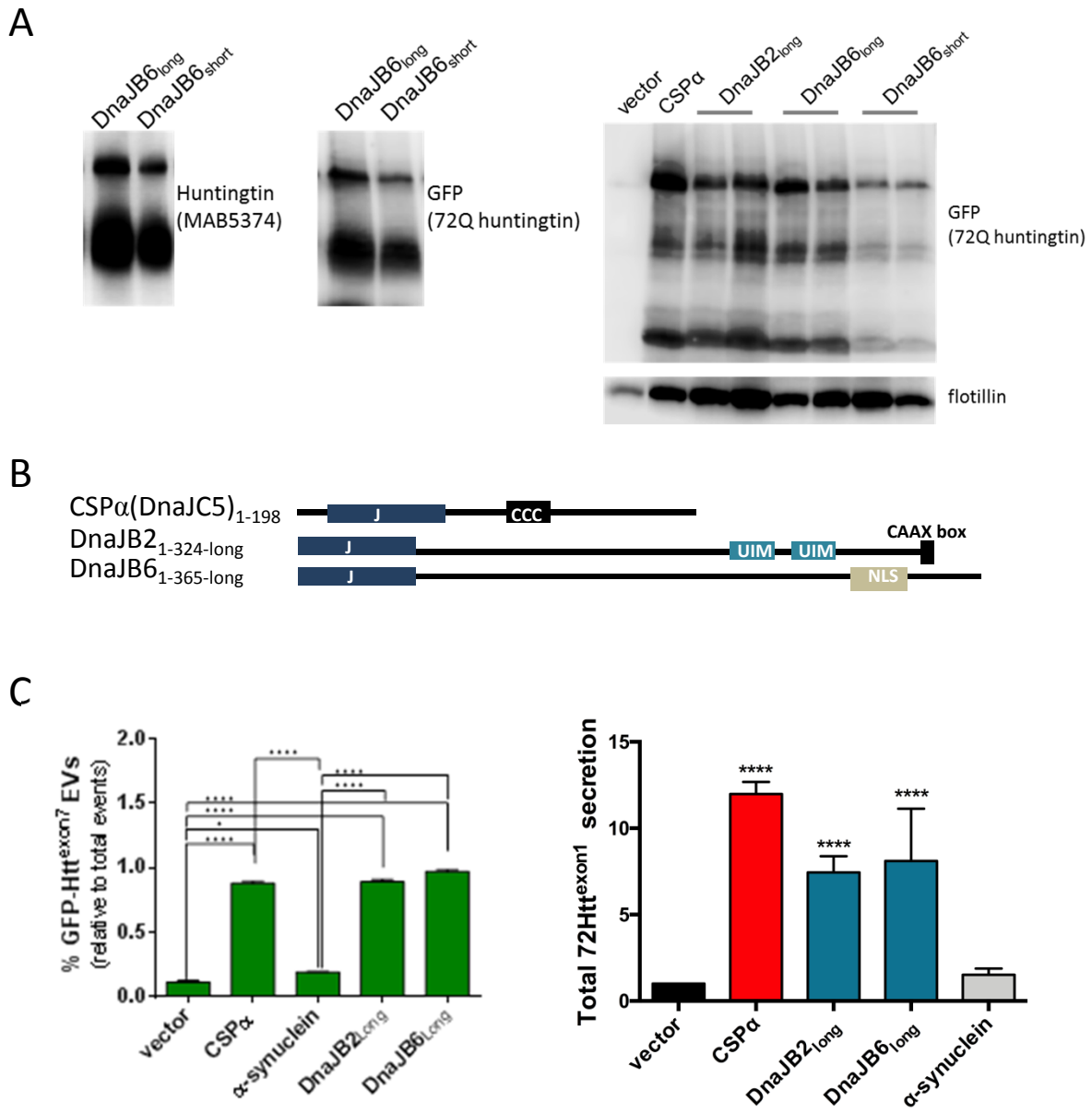
A
DnaJB6long
DnaJB6short
Huntingtin
(MAB5374)
GFP
(72Q huntingtin)
vector
CSPα
DnaJB2long
flotillin
B
CSPα(DnaJC5)1-198
DnaJB21-324-long
DnaJB61-365-long
J
CCC
UIM
NLS
CAAX box
C
% GFP-Httexon7 EVs
(relative to total events)
Total 72Httexon1 secretion
α-synuclein

Figure 6.

Reference List

[1] L. Alvarez-Erviti*, et al.*, "Lysosomal dysfunction increases exosome-mediated alpha-synuclein release and transmission," Neurobiol. Dis. **42**(3), 360 (2011).

[2] F. A. Aprile*, et al.*, "The molecular chaperones DNAJB6 and Hsp70 cooperate to suppress alpha-synuclein aggregation," Sci. Rep. **7**(1), 9039 (2017).

[3] B. A. Benitez*, et al.*, "Exome-sequencing confirms DNAJC5 mutations as cause of adult neuronal ceroid-lipofuscinosis," PLoS. ONE. **6**(11), e26741 (2011).

[4] S. C. Blumen*, et al.*, "A rare recessive distal hereditary motor neuropathy with HSJ1 chaperone mutation," Ann. Neurol **71**(4), 509 (2012).

[5] J. E. Braun and R. H. Scheller, "Cysteine string protein, a DnaJ family member, is present on diverse secretory vesicles," **34**(11), 1361 (1995).

[6] J. E. Braun, S. M. Wilbanks, and R. H. Scheller, "The cysteine string secretory vesicle protein activates Hsc70 ATPase," J Biol Chem **271**(42), 25989 (1996).

[7] S. Chandra*, et al.*, "Alpha-synuclein cooperates with CSPalpha in preventing neurodegeneration," **123**(3), 383 (2005).

[8] J. P. Chapple and M. E. Cheetham, "The chaperone environment at the cytoplasmic face of the endoplasmic reticulum can modulate rhodopsin processing and inclusion formation," J Biol Chem **278**(21), 19087 (2003).

[9] J. P. Chapple*, et al.*, "Neuronal DnaJ proteins HSJ1a and HSJ1b: a role in linking the Hsp70 chaperone machine to the ubiquitin-proteasome system?," Biochem. Soc. Trans. **32**(Pt 4), 640 (2004).

[10] M. E. Cheetham, J. P. Brion, and B. H. Anderton, "Human homologues of the bacterial heat-shock protein DnaJ are preferentially expressed in neurons," Biochem. J **284 (Pt 2)**, 469 (1992).

[11] H. J. Chen*, et al.*, "The heat shock response plays an important role in TDP-43 clearance: evidence for dysfunction in amyotrophic lateral sclerosis," Brain **139**(Pt 5), 1417 (2016).

[12] J. Z. Chuang*, et al.*, "Characterization of a brain-enriched chaperone, MRJ, that inhibits huntingtin aggregation and toxicity independently," J Biol Chem **277**(22), 19831 (2002).

[13] F. Cicchetti*, et al.*, "Mutant huntingtin is present in neuronal grafts in Huntington disease patients," Ann. Neurol. **76**(1), 31 (2014).

[14] M. Costanzo*, et al.*, "Transfer of polyglutamine aggregates in neuronal cells occurs in tunneling nanotubes," J. Cell Sci. **126**(Pt 16), 3678 (2013).

[15] J. Deng*, et al.*, "Neurons Export Extracellular Vesicles Enriched in Cysteine String Protein and Misfolded Protein Cargo," Sci. Rep. **7**(1), 956 (2017).

[16] J. Donnelier*, et al.*, "Increased Expression of the Large Conductance, Calcium-Activated K+ (BK) Channel in Adult-Onset Neuronal Ceroid Lipofuscinosis," PLoS. ONE. **10**(4), e0125205 (2015).

[17] P. F. Durrenberger*, et al.*, "DnaJB6 is present in the core of Lewy bodies and is highly up-regulated in parkinsonian astrocytes," J. Neurosci. Res. **87**(1), 238 (2009).

[18] E. Emmanouilidou, L. Stefanis, and K. Vekrellis, "Cell-produced alpha-synuclein oligomers are targeted to, and impair, the 26S proteasome," Neurobiol. Aging **31**(6), 953 (2010).

[19] Z. Fayazi*, et al.*, "A Drosophila ortholog of the human MRJ modulates polyglutamine toxicity and aggregation," Neurobiol Dis. **24**(2), 226 (2006).

[20] R. Fernandez-Chacon*, et al.*, "The synaptic vesicle protein CSP alpha prevents presynaptic degeneration," **42**(2), 237 (2004).

[21] B. Fevrier*, et al.*, "Cells release prions in association with exosomes," Proc Natl Acad Sci U S A **101**(26), 9683 (2004).

[22] S. N. Fontaine*, et al.*, "DnaJ/Hsc70 chaperone complexes control the extracellular release of neurodegenerative-associated proteins," EMBO J. **35**(14), 1537 (2016).

[23] X. C. Gao*, et al.*, "Co-chaperone HSJ1a dually regulates the proteasomal degradation of ataxin-3," PLoS. ONE. **6**(5), e19763 (2011).

[24] J. C. Genereux*, et al.*, "Unfolded protein response-induced ERdj3 secretion links ER stress to extracellular proteostasis," EMBO J. **34**(1), 4 (2015).

[25] B. Gess*, et al.*, "HSJ1-related hereditary neuropathies: novel mutations and extended clinical spectrum," Neurology **83**(19), 1726 (2014).

[26] J. Gillis*, et al.*, "The DNAJB6 and DNAJB8 protein chaperones prevent intracellular aggregation of polyglutamine peptides," J. Biol. Chem. **288**(24), 17225 (2013).

[27] C. Gomes*, et al.*, "Evidence for secretion of Cu,Zn superoxide dismutase via exosomes from a cell model of amyotrophic lateral sclerosis," Neurosci. Lett. **428**(1), 43 (2007).

[28] E. L. Gorenberg and S. S. Chandra, "The Role of Co-chaperones in Synaptic Proteostasis and Neurodegenerative Disease," Front Neurosci. **11**, 248 (2017).

[29] L. I. Grad*, et al.*, "Exosome-dependent and independent mechanisms are involved in prion-like transmission of propagated Cu/Zn superoxide dismutase misfolding," Prion. **8**(5), 331 (2014).

[30] L. I. Grad*, et al.*, "Intercellular propagated misfolding of wild-type Cu/Zn superoxide dismutase occurs via exosome-dependent and -independent mechanisms," Proc. Natl. Acad. Sci. U. S. A **111**(9), 3620 (2014).

[31] J. F. Gusella and M. E. MacDonald, "Molecular genetics: unmasking polyglutamine triggers in neurodegenerative disease," Nat. Rev. Neurosci. **1**(2), 109 (2000).

[32] J. Hageman*, et al.*, "A DNAJB chaperone subfamily with HDAC-dependent activities suppresses toxic protein aggregation," Mol. Cell **37**(3), 355 (2010).

[33] M. B. Harms*, et al.*, "Exome sequencing reveals DNAJB6 mutations in dominantly-inherited myopathy," Ann. Neurol. **71**(3), 407 (2012).

[34] M. X. Henderson*, et al.*, "Neuronal ceroid lipofuscinosis with DNAJC5/CSPalpha mutation has PPT1 pathology and exhibit aberrant protein palmitoylation," Acta Neuropathol. **131**(4), 621 (2016).

[35] J. L. Howarth*, et al.*, "Hsp40 molecules that target to the ubiquitin-proteasome system decrease inclusion formation in models of polyglutamine disease," Mol. Ther. **15**(6), 1100 (2007).

[36] J. Howitt and A. F. Hill, "Exosomes in the Pathology of Neurodegenerative Diseases," J. Biol. Chem. **291**(52), 26589 (2016).

[37] V. Kakkar*, et al.*, "The S/T-Rich Motif in the DNAJB6 Chaperone Delays Polyglutamine Aggregation and the Onset of Disease in a Mouse Model," Mol. Cell (2016).

[38] V. Kakkar, L. C. Prins, and H. H. Kampinga, "DNAJ proteins and protein aggregation diseases," Curr. Top. Med. Chem. **12**(22), 2479 (2012).

[39] H. Kalra, G. P. Drummen, and S. Mathivanan, "Focus on Extracellular Vesicles: Introducing the Next Small Big Thing," Int. J. Mol. Sci. **17**(2), 170 (2016).

[40] H. H. Kampinga and E. A. Craig, "The HSP70 chaperone machinery: J proteins as drivers of functional specificity," Nat Rev Mol. Cell Biol **11**(8), 579 (2010).

[41] S. S. Kashyap*, et al.*, "Caenorhabditis elegans dnj-14, the orthologue of the DNAJC5 gene mutated in adult onset neuronal ceroid lipofuscinosis, provides a new platform for neuroprotective drug screening and identifies a SIR-2.1-independent action of resveratrol," Hum. Mol. Genet. **23**(22), 5916 (2014).

[42] S. S. Kashyap*, et al.*, "Caenorhabditis elegans dnj-14, the orthologue of the DNAJC5 gene mutated in adult onset neuronal ceroid lipofuscinosis, provides a new platform for neuroprotective drug screening and identifies a SIR-2.1-independent action of resveratrol," Hum. Mol. Genet. (2014).

[43] C. Koutras and J. E. Braun, "J protein mutations and resulting proteostasis collapse," Front Cell Neurosci. **8**, 191 (2014).

[44] B. D. Kyle*, et al.*, "The Large Conductance, Calcium-activated K(+) (BK) Channel is regulated by Cysteine String Protein," Sci. Rep. **3**, 2447 (2013).

[45] J. Labbadia*, et al.*, "Suppression of protein aggregation by chaperone modification of high molecular weight complexes," Brain **135**(Pt 4), 1180 (2012).

[46] S. L. Maas, X. O. Breakefield, and A. M. Weaver, "Extracellular Vesicles: Unique Intercellular Delivery Vehicles," Trends Cell Biol. **27**(3), 172 (2017).

[47] C. Mansson*, et al.*, "Interaction of the molecular chaperone DNAJB6 with growing amyloid-beta 42 (Abeta42) aggregates leads to sub-stoichiometric inhibition of amyloid formation," J. Biol. Chem. **289**(45), 31066 (2014).

[48] L. Maroteaux, J. T. Campanelli, and R. H. Scheller, "Synuclein: a neuron-specific protein localized to the nucleus and presynaptic nerve terminal," J Neurosci **8**(8), 2804 (1988).

[49] I. Melentijevic*, et al.*, "C. elegans neurons jettison protein aggregates and mitochondria under neurotoxic stress," **542**(7641), 367 (2017).

[50] L. C. Miller*, et al.*, "Cysteine String Protein (CSP) inhibition of N-type calcium channels is blocked by mutant huntingtin," J Biol Chem **278**, 53072 (2003).

[51] A. Mitra*, et al.*, "Large isoform of MRJ (DNAJB6) reduces malignant activity of breast cancer," Breast Cancer Res. **10**(2), R22 (2008).

[52] R. I. Morimoto, "Proteotoxic stress and inducible chaperone networks in neurodegenerative disease and aging," Genes Dev. **22**(11), 1427 (2008).

[53] T. Nonaka*, et al.*, "Prion-like properties of pathological TDP-43 aggregates from diseased brains," Cell Rep. **4**(1), 124 (2013).

[54] L. Noskova*, et al.*, "Mutations in DNAJC5, encoding cysteine-string protein alpha, cause autosomal-dominant adult-onset neuronal ceroid lipofuscinosis," Am. J Hum. Genet **89**(2), 241 (2011).

[55] S. S. Novoselov*, et al.*, "Molecular chaperone mediated late-stage neuroprotection in the SOD1(G93A) mouse model of amyotrophic lateral sclerosis," PLoS. ONE. **8**(8), e73944 (2013).

[56] T. Ohyama*, et al.*, "Huntingtin-interacting protein 14, a palmitoyl transferase required for exocytosis and targeting of CSP to synaptic vesicles," J Cell Biol **179**(7), 1481 (2007).

[57] J. Palmio*, et al.*, "Novel mutations in DNAJB6 gene cause a very severe early-onset limb-girdle muscular dystrophy 1D disease," Neuromuscul. Disord. **25**(11), 835 (2015).

[58] J. C. Polanco*, et al.*, "Extracellular Vesicles Isolated from the Brains of rTg4510 Mice Seed Tau Protein Aggregation in a Threshold-dependent Manner," J. Biol. Chem. **291**(24), 12445 (2016).

[59] L. Rajendran*, et al.*, "Alzheimer's disease beta-amyloid peptides are released in association with exosomes," Proc. Natl. Acad. Sci. U. S. A **103**(30), 11172 (2006).

[60] J. M. Rose*, et al.*, "Molecular chaperone-mediated rescue of mitophagy by a Parkin RING1 domain mutant," Hum. Mol. Genet. **20**(1), 16 (2011).

[61] E. Sanchez*, et al.*, "Identification of a Large DNAJB2 Deletion in a Family with Spinal Muscular Atrophy and Parkinsonism," Hum. Mutat. **37**(11), 1180 (2016).

[62] J. Sarparanta, *et al.*, "Mutations affecting the cytoplasmic functions of the co-chaperone DNAJB6 cause limb-girdle muscular dystrophy," Nat. Genet. **44**(4), 450 (2012).

[63] T. Sato, *et al.*, "DNAJB6 myopathy in an Asian cohort and cytoplasmic/nuclear inclusions," Neuromuscul. Disord. **23**(3), 269 (2013).

[64] R. A. Sharples, *et al.*, "Inhibition of gamma-secretase causes increased secretion of amyloid precursor protein C-terminal fragments in association with exosomes," FASEB J. **22**(5), 1469 (2008).

[65] B. Shen, *et al.*, "Protein targeting to exosomes/microvesicles by plasma membrane anchors," J. Biol. Chem. **286**(16), 14383 (2011).

[66] R. A. Stern, *et al.*, "Preliminary Study of Plasma Exosomal Tau as a Potential Biomarker for Chronic Traumatic Encephalopathy," J. Alzheimers. Dis. **51**(4), 1099 (2016).

[67] G. Suarez-Cedeno, T. Winder, and M. Milone, "DNAJB6 myopathy: A vacuolar myopathy with childhood onset," Muscle Nerve **49**(4), 607 (2014).

[68] T. Takeuchi, *et al.*, "Intercellular chaperone transmission via exosomes contributes to maintenance of protein homeostasis at the organismal level," Proc. Natl. Acad. Sci. U. S. A **112**(19), E2497-E2506 (2015).

[69] S. S. Tiwari, *et al.*, "Evidence that the presynaptic vesicle protein CSPalpha is a key player in synaptic degeneration and protection in Alzheimer's disease," Mol. Brain **8**(1), 6 (2015).

[70] M. Velinov, *et al.*, "Mutations in the Gene DNAJC5 Cause Autosomal Dominant Kufs Disease in a Proportion of Cases: Study of the Parry Family and 8 Other Families," PLoS. ONE. **7**(1), e29729 (2012).

[71] L. J. Vella, *et al.*, "Enrichment of prion protein in exosomes derived from ovine cerebral spinal fluid," Vet. Immunol. Immunopathol. **124**(3-4), 385 (2008).

[72] L. J. Vella, A. F. Hill, and L. Cheng, "Focus on Extracellular Vesicles: Exosomes and Their Role in Protein Trafficking and Biomarker Potential in Alzheimer's and Parkinson's Disease," Int. J. Mol. Sci. **17**(2), 173 (2016).

[73] E. D. Watson, *et al.*, "The Mrj co-chaperone mediates keratin turnover and prevents the formation of toxic inclusion bodies in trophoblast cells of the placenta," Development **134**(9), 1809 (2007).

[74] B. Westhoff, *et al.*, "HSJ1 is a neuronal shuttling factor for the sorting of chaperone clients to the proteasome," Curr. Biol **15**(11), 1058 (2005).

[75] C. Zarouchlioti, *et al.*, "DNAJ Proteins in neurodegeneration: essential and protective factors," Philos. Trans. R. Soc. Lond B Biol. Sci. **373**(1738) (2018).

[76] Y. Q. Zhang, *et al.*, "Identification of CSPalpha Clients Reveals a Role in Dynamin 1 Regulation," **74**(1), 136 (2012).

[77] K. E. Zinsmaier, *et al.*, "Paralysis and early death in cysteine string protein mutants of Drosophila," **263**(5149), 977 (1994).

Supplementary Plasmid Information

The amino acid sequence of mouse CSPα (DnaJC5) is (198aa, NP 058055.1):
madqrqrslstsgeslyhvlgldknatsddikksyrklalkyhpdknpdnpeaadkfkeinnahailtdatkrniydkygslglyvaeqf
geenvntyfvlsswwakalfvvcglltccyccccclcccfncccgkckpkapegeetefyvspedleaqlqsdereatdtpiviqpasate
ttqltadshpsyhtdgfn

The amino acid sequence of mouse DnaJB2 (HSJ1) is (324aa, NM_001159883):
masyyeildvprsaspddikkayryyalqwhpdknpdnkefaekkfkevaeayevlsdkhkreiydrygregltgagsgpsrsetgg
agpgftftfrspeevfreffgsgdpfselfddlgvfselqnqgprltgpfftfsssfpansdfssssfsfspggagfrsvststtfvqgrrittrri
mengqerveveedgqlksvsingvpddlalglelsrreqqpsvapglgvmqurptslsrppdhdlsededlqlamayslsemeaag
qkpaggrgaqqrqhgqpkaqhrdldvggthksvrgeaaklspsseekasrchil

The amino acid sequence of mouse DnaJB6short (mrj) is (242aa, NP_035977.2):
mvdyyevlgvqrhaspedikkayrkqalkwhpdknpenkeeaerkfkqvaeayevlsdakkrdiydkygkeglngggggggihfd
spfefgftfrnpddvfreffggrdpfsfdffedpfddffgnrrgprgnrsrgagsffstfsgfpsfgsgfpafdtgftpfgslghggltsfsstsf
ggsgmgnfksiststkivngkkittkrivengqerveveedgqlksltingkehllrldnk

The amino acid sequence of mouse DnaJB6LONG (mrj) is (365aa, NM_001037940.4)
mvdyyevlgvqrhaspedikkayrkqalkwhpdknpenkeeaerkfkqvaeayevlsdakkrdiydkygkeglngggggggihfd
spfefgftfrnpddvfreffggrdpfsfdffedpfddffgnrrgprgnrsrgagsffstfsgfpsfgsgfpafdtgftpfgslghggltsfsstsf
ggsgmgnfksiststkivngkkittkrivengqerveveedgqlksltingvadenalaeecqrrgqptpalapgpapapvrvpsqarp
laptpaptpaptpapapaqtpapsvstrpqkpprpaptaklgsksnweddeqdrqrvpgnwdapmtsaglkeggkrkkqkqke
dlkkkkstkgnh

The amino acid sequence of rat DnaJB1 is (340aa, BC159430.1):
mgkdyyqtlglargasddeikrayrrqalryhpdknkepgaeekfkeiaeaydvlsdprkreifdrygeeglkgggpsggssggangt
sfsytfhgdphamfaeffggrnpfdtffgqrngeegmdiddpfssfpmgmggftnmnfgrsrptqeptrkkqdppvthdlrvslee
iysgctkkmkishkrlnpdgksirnedkiltievkrgwkegtkitfpkegdqtsnnipadivfvlkdkphnifkrdgsdviyparislrealc
gctvnvptldgrtipvvfkdvirpgmrrkvpgeglplpktpekrgdlviefevifpdripissrtileqvlpi

The amino acid sequence of mouse DnaJB11 is (358aa,NP_080676.3):
mapqnlstfcllllyligtviagrdgykilgvprsasikdikkayrklalqlhpdrnpddpqaqekfqdlgaayevlsdsekrkqydtygee
glkdghqsshgdifshffgdfgfmfggtprqqdrniprgsdiivdlevtleevyagnfvevvrnkpvarqapgkrkcncrqemrttqlg
pgrfqmtqevvcdecpnvklvneertleveiepgvrdgmeypfigegephvdgepgdlrfrikvvkhriferrgddlytnvtvslveal
vgfemdithldghkvhisrdkitrpgaklwkkgeglpnfdnnnikgsliitfdvdfpkeqlteeakegikqllkqgpvqkvynglqgy

The amino acid sequence of mouse DnaJA1 is (397aa, NP_032324.1):
mvkettyydvlgvkpnatqeelkkayrklalkyhpdknpnegekfkqisqayevladskkrelydkggeqaikeggagggfgspmd
ifdmffggggrmqrerrgknvvhqlsvtledlyngatrklalqknvicdkcegrggkkgaveccpncrgtgmqirihqigpgmvqqiq
svcmecqghgerispkdrckscngrkivrekkilevhidkgmkdgqkitfhgegdqepglepgdiiivldqkdhavftrrgedlfmcm
diqlvealcgfqkpistldnrtivitshpgqivkhgdikcvlnegmpiyrrpyekgrliiefkvnfpengflspdklsllekllperkeveetd
emdqvelvdfdpnqerrrhyngeayeddehhprggvqcqts

The amino acid sequence of mouse DnaJC13 is (2243aa, NP_001156498.1):
mniirenkdlacfyttkhswrgkykrvfsvgthavttynpntlevtnqwpygdicsispvgkgqgtefnltfrkgsgkksetlkfstehrt
elltealrfrtdfaegkitgrryncykhhwsdakkpvvlevtpggfdqinpvtnrvlcsydyrniegfvdlsdyqggfcilyggfsrlhlfsse
qreeiiksaiehagnyigislrirkeplefeqylnlrfgkystdesitslaefvvqkisprhsepvkrvlavtetclverdpatyniatlkplgev
falvcdsenpqlftiefikgqvrkyssterdsllaslldgvrasgnrdvcvkmapthkgqrwgllsmpideeveslhlrflaappngnfad
avfrfnanisysgvlhavtqdglfsenkeklinnaitallsqegdvvasnaelesqfqavrrlvaskagflaftqlpkfrerlgmkvvkalkr
snngvihaavdmlcalmcpmhddydlrqeqlnkasllsskkflenllekfnshvdhgtgalvisslldfltfalcapysettegqqfdmll
emvasngrtlfklfqhpsmaivkgaglvmkaiieegdreiatkmqelalsegalprhlhtamftissdqrmltnrqlsrhlvglwtadn
ttatnllkrilppgllayldssdpvpekdadrmhvrdnvkiamdqygkfnkvpewqrlagkaakevekfakekvdlvlmhwrdrmg
iaqkeninqkpvvlrkrrqrikieanwdlfyyrfsqdharsnliwnfktreelkdalesemrtfnidrelgsasviswnhhefevkyecla
eeikigdyylrllleedeneesgsikrsyeffnelyhrflltpkvnmkclclqalaivygrcheeigpftdtryiigmlerctdklerdrlilflnk
lilnkknvkdlmdsngirilvdlltlahlhvsratvplqsnvieaspdmkresekewyfgnadkersgpygfhemqelwakgmlnakt
rcwaqgmdgwrplqaipqlkwcllasgqavlnetdlatlilnmlitmcgyfpsrdqdnaiirplprvkrllsdstclphviqllltfdpilve
kvaillhhimqdnpqlprlylsgvfffimmytgsnvlpvarflkythskqafkseetkgqdifqrsilghilpeamvcylenyepekfseif
lgefdtpeaiwssemrrlmiekiaahladftprlqsntralyqycpipvinypqlenelfcniyylkqlcdtlrfpdwpikdpvkllkdsld
awkkevekkppmmsiddayevlnlpigqglhdeskirkayfrlaqkyhpdknpegrdmfekvnkayeflctkstkivdgpdpeniil
ilktqsilfnrhkeelqpykyagypmlirtitmetsddllfskespllpaaaelafhtvncsalnaeelrrenglevlqeafsrcvavlnrssk
psdmsvqvcghisrcysvaaqfeecrekitempgiikdlcrvlyfgkciprvaalavecvssfavdfwlqthlfqagilwyllvylfnydyt
leesgiqkneetnqqevanslaklsvhalsrlggylsedqatpenptvrkslagmltpyiarklavasatetlkmlnsntespylmwnn
straelleflesqqenmikkgdcdktygaefvysehakelivgeifvrvynevptfqlevpkefaaslldyigsqaqylhtfmaithaakv
eseqhgdrlprvemalealrnvikynpgsesecighfklifsllrvhgagqvqqlalevvnivtsnqdcvnniaesmvlsnllallhslpss
rqlvletlyalasntkiikeamakgaliylldmfcnsthpqvrsqtaelfakmtadkligpkvritlmkflpsvfmdamrdnpeaavhif
egthenpeliwndssrdkvsttvremmlehfknqrdnpdvnwklpedfavvfgeaegelavggvflrifiaqpawvlrkpreflialle
kltelleknnphgetletltmatvclfsaqpqladqvpplghlpkviqamnhrnnaipksairvihvlsdnelcvramasletigplmng
mrkradtvglaceainrmfqkeqselvaqalkaelvpyllkllegvglenldspaatkaqivkalkamtrslqygeqvseilsrssvwsaf
kdqkhdlfisdsqtagyltgpgvagyltagtsssamsnlpppvdheagdlgyqt

The amino acid sequence for mouse DnaJC19 is (116aa, NP_080608.3):
mastvvavgltiaaagfagryvlqamkhvepqvkqvfqslpksafgggyyrggfepkmtkreaalilgvsptankgkirdahrrimlln
hpdkggspyiaakineakdllegqakk

The amino acid sequence for mouse DnaJC14 is (703aa, NP_083149.3):
maqkhpgerrlcgahrsggtslstsgssvdpeilsfsglrdsaetapngtrclkehsgpkytqppnpahwsdpshgpprgpgpprgg
gypdesetgseesgvdqelsrenetgyqedgspsflsipsacncqgspgvpegtyseegdgsssslchhctspalgedeeleeeydd
eeplkfpsdfsrvssgkkplsrrqkhrflikedvrdsgrrepkapgrhrlarkrsqtdkrrglglwgveelcqlgqagfwwliellvlvgeyv
etcghliyacrklkgsdldlfrvwvgvwarrlggwarmmfqflsqsffcvvglliril rvvgafllalalflgclqlgwrfsvglgnrlgwrdkt
awlfswlgspalhhcltllkdsrpwqqlvrliqwgwqelpwvkqrtkkqgnapvasgrycqpeeevtrlltmagvpedelnpfhvlg
veatasdtelkkayrqlavmvhpdknhhpraeeafkilraawdivsnperrkeyemkrmaenelsrsvneflsklqddlkeamnt
mmcsrcqgkhrrfemdrepksarycaecnrlhpaeegdfwaessmlglkityfalmdgkvyditewagcqrvgispdthrvpyhi
sfgsrvpgtsgrqratpesppadlqdflsrifqvppgpmsngnffaaphpgpgttstsrpnssvpkgeakpkrrkkvrrpfqr

The amino acid sequence for rat α-synuclein is (140aa, NP_062042.1):
mdvfmkglskakegvvaaaektkqgvaeaagktkegvlyvgsktkegvvhgvttvaektkeqvtnvggavvtgvtavaqktvega
gniaaatgfvkkdqmgkgeegypqegiledmpvdpsseayempseegyqdyepea

Supplementary Antibody Information.

Anti CSP polyclonal	(Braun and Scheller, 1995)
Anti-actin monoclonal	Sigma-Aldrich
Anti-flotillin-1 monoclonal	BD Transduction Labs
Anti-DnaJB1 polyclonal	Thermo Fisher Scientific
Anti-DnaJB2 polyclonal	Sigma-Aldrich
Anti-DnaJB6 polyclonal	Thermo Fisher Scientific
Anti-DnaJB11 polyclonal	Cedarlane
Anti-DnaJA1 monoclonal	Cedarlane
Anti-C13 polyclonal	Cedarlane
Anti-C14 polyclonal	Abcam
Anti-α-synuclein monoclonal	Cedarlane
Anti-huntingtin-5374	Millipore
Anti-GFP polyclonal	Santa Cruz Biotechnology

Supplementary Figures

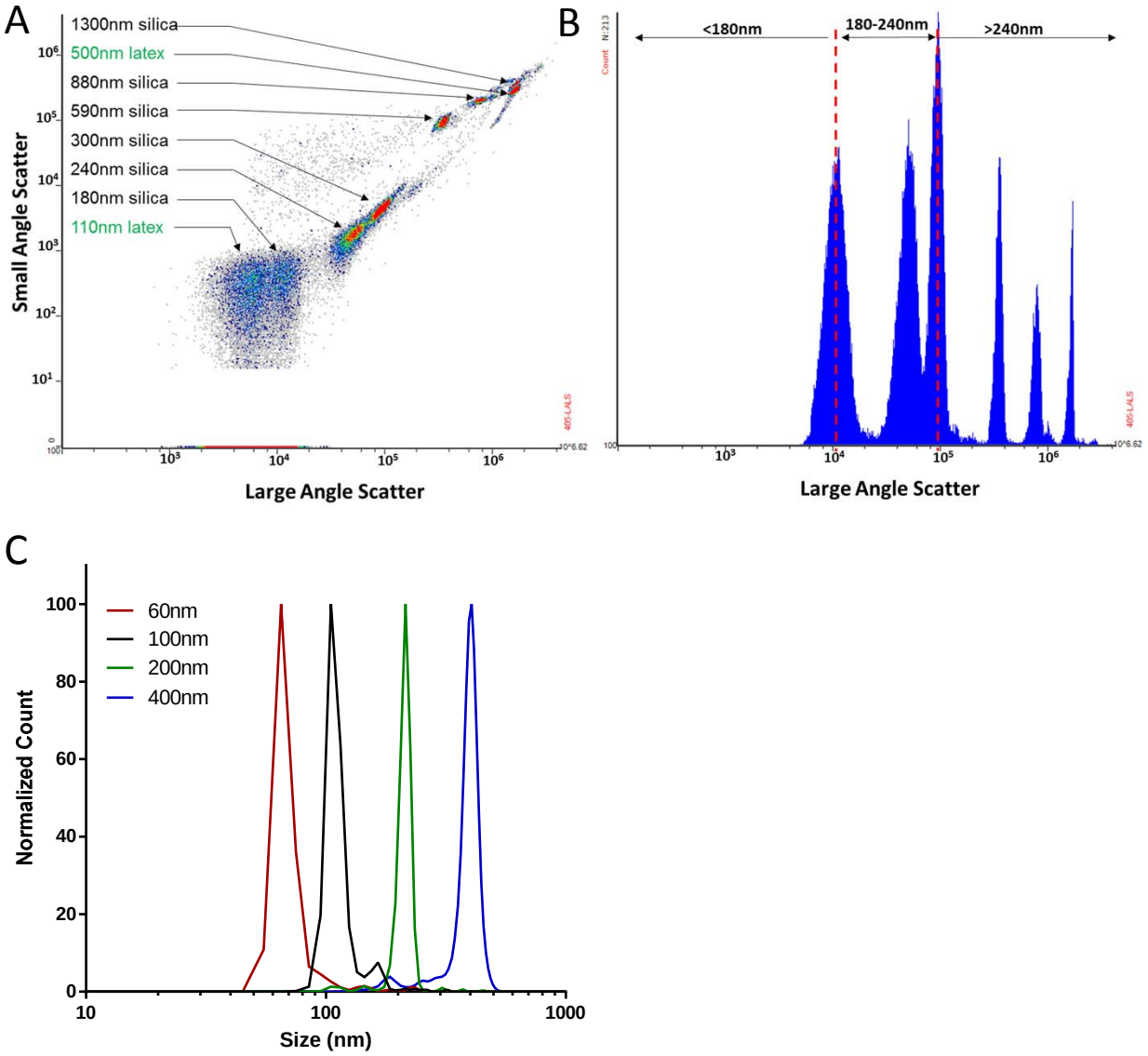

Supplementary Figure 1.

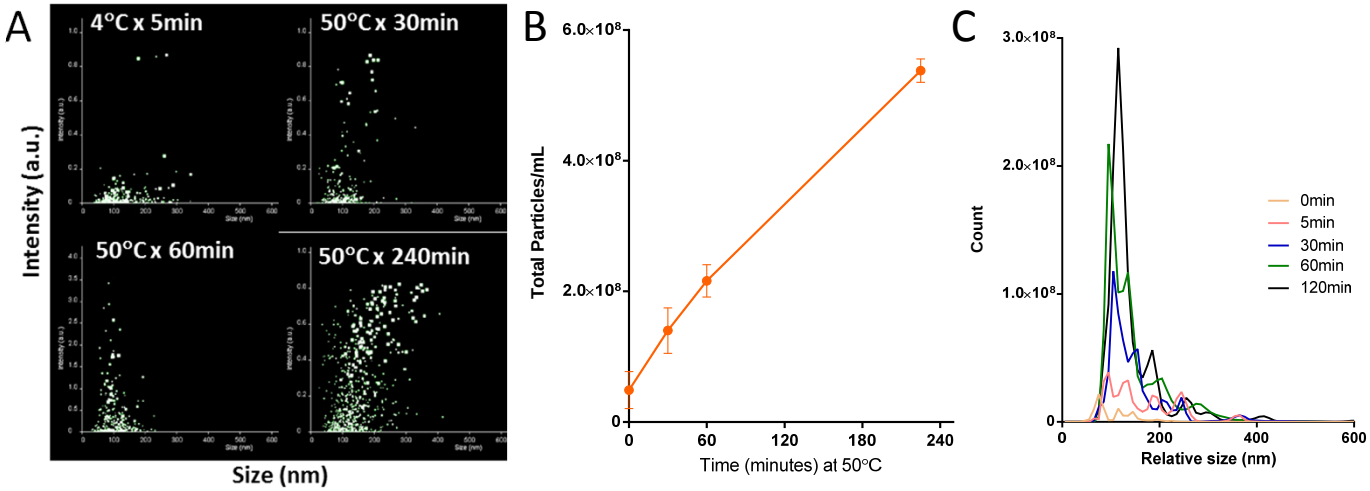

Supplementary Figure 2.

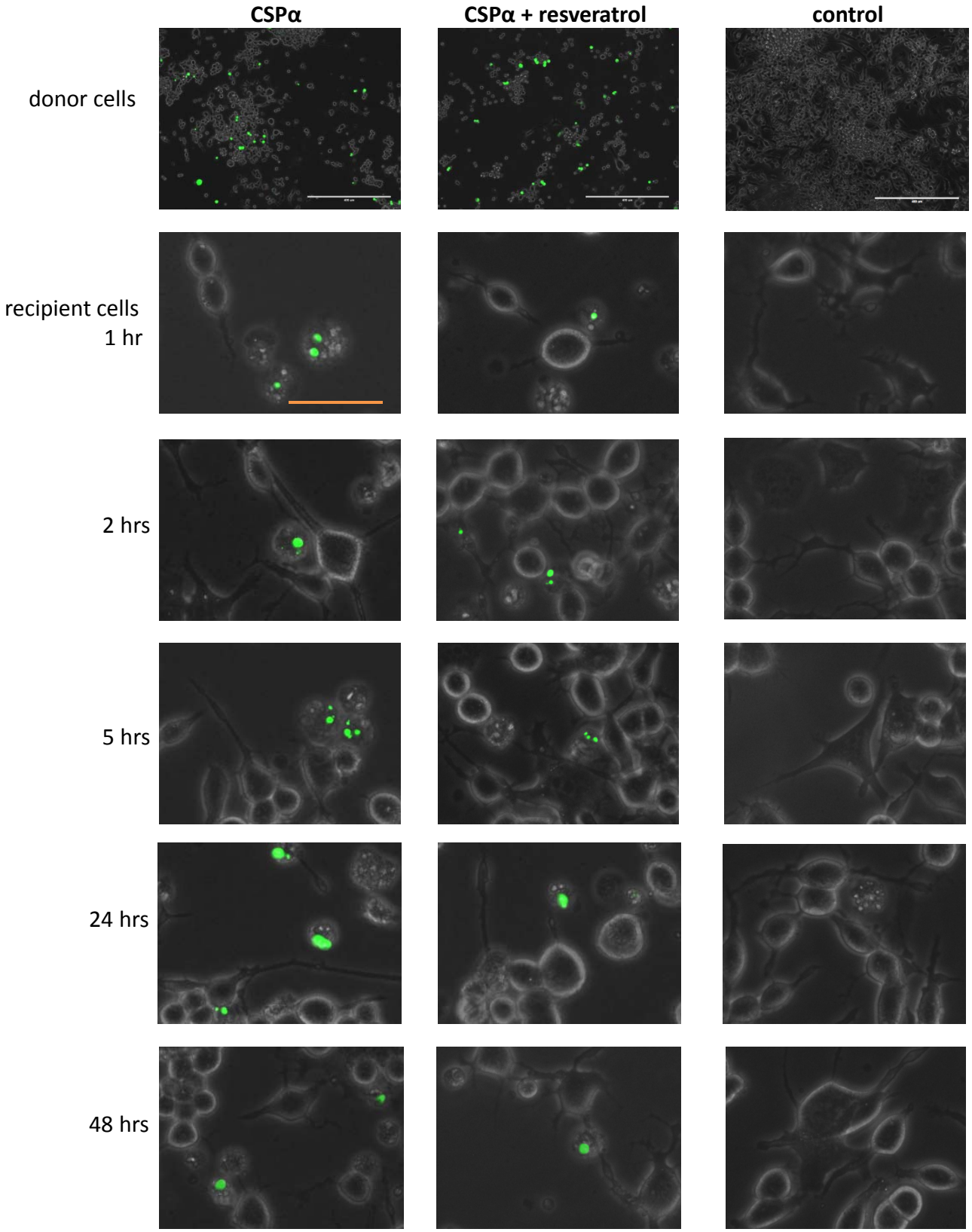

Supplementary Figure 3.

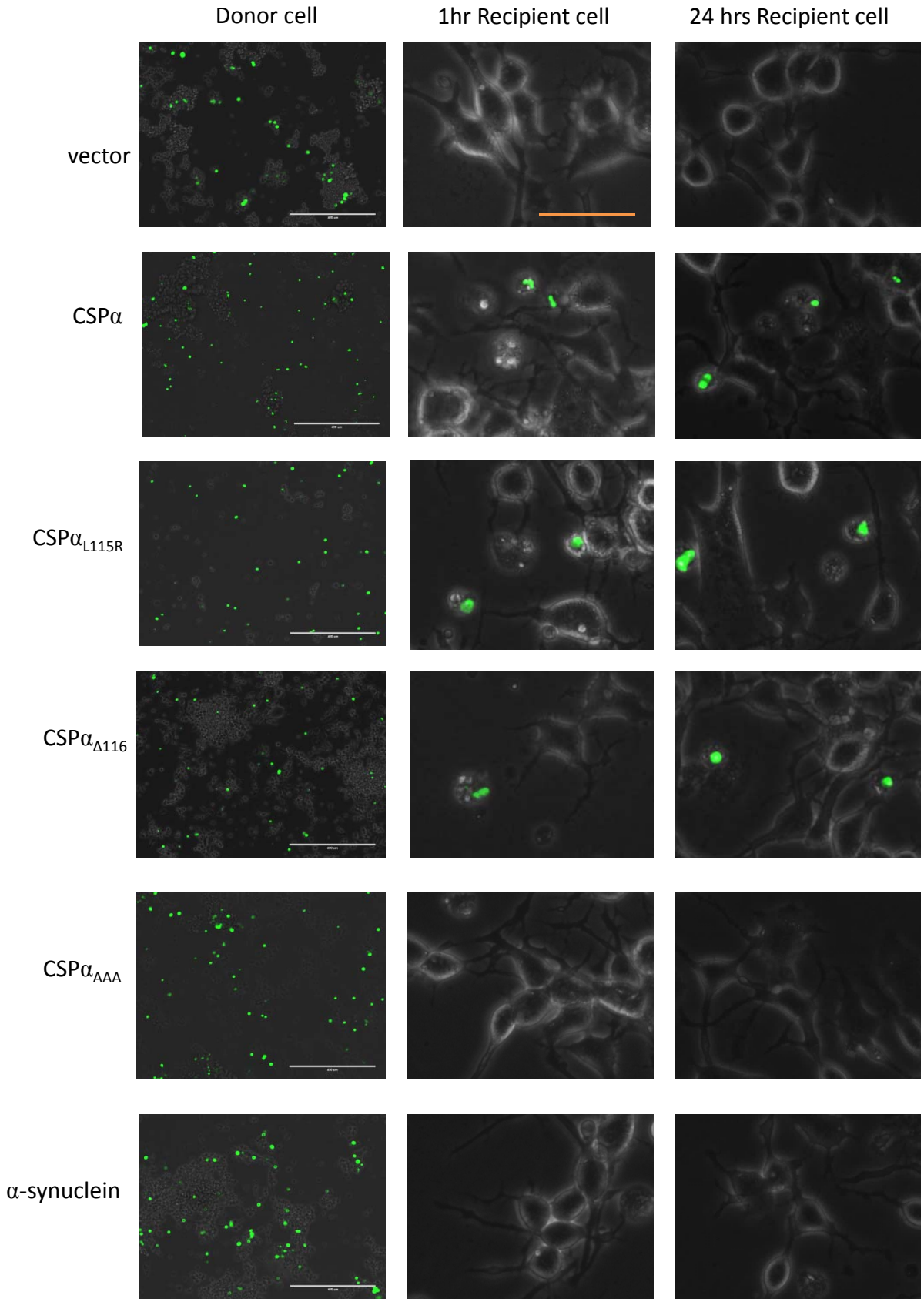

Supplementary Figure 4.

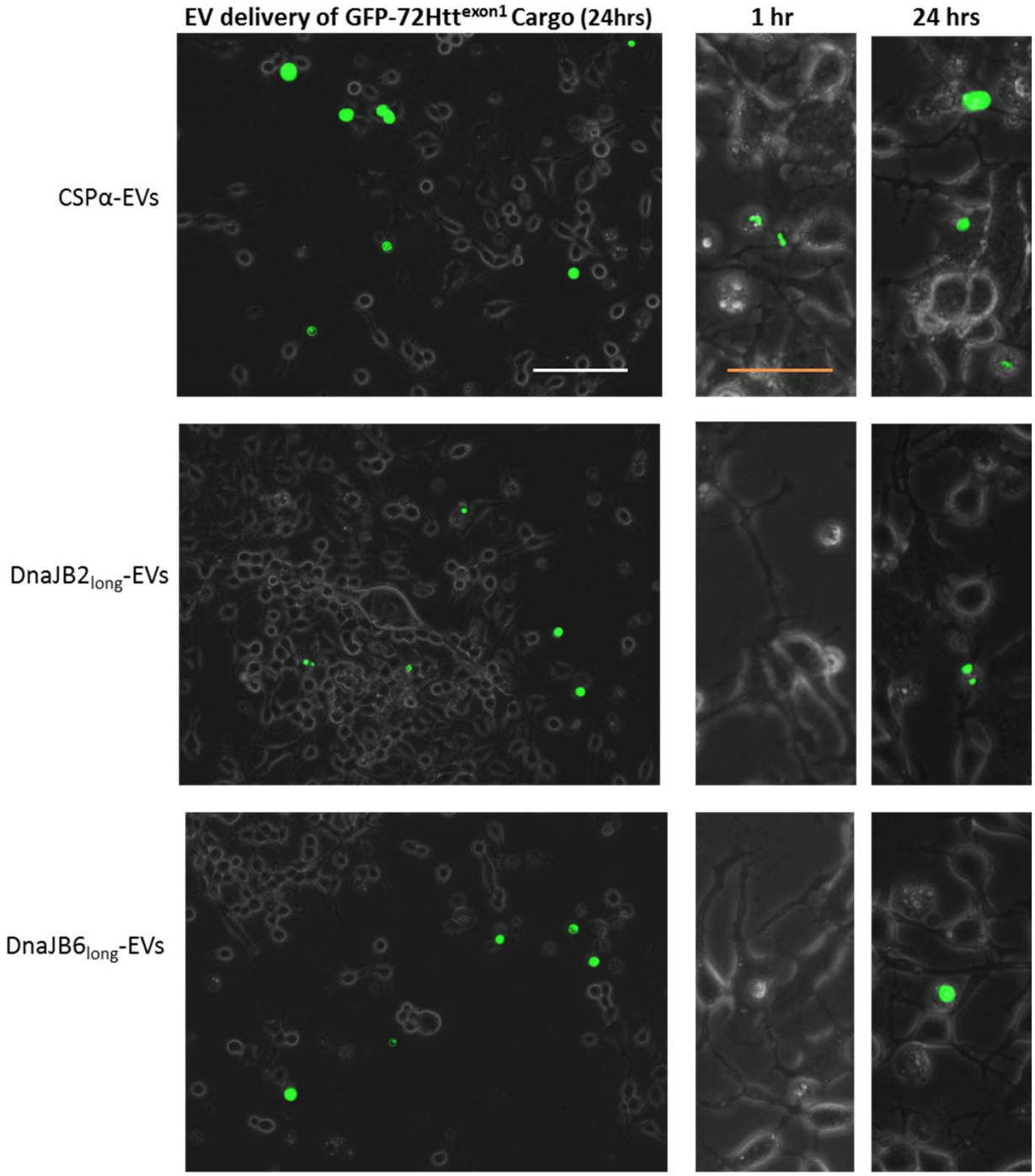

Supplementary Figure 5.